Seasonal water mass evolution and non-Redfield dynamics enhance CO_2 uptake in the Chukchi Sea

Zhangxian Ouyang[1], Andrew Collins[1,2], Yun Li[1], Di Qi[3,4], Kevin R. Arrigo[5], Yanpei Zhuang[3,6], Shigeto Nishino[7], Matthew P. Humphreys[8], Naohiro Kosugi[9], Akihiko Murata[10], David L. Kirchman[1], Liqi Chen[4], Jianfang Chen[6], Wei-Jun Cai[1]*

[1] School of Marine Science and Policy, University of Delaware, Newark, Delaware, USA
[2] NOAA Pacific Marine Environmental Laboratory, Seattle, WA, USA
[3] Polar and Marine Research Institute, Jimei University, Xiamen, China
[4] Key Laboratory of Global Change and Marine-Atmospheric Chemistry of Ministry of Natural Resources, Third Institute of Oceanography, MNR, Xiamen 361005, China
[5] Department of Earth System Science, Stanford University, Stanford, CA 94305, USA
[6] Key Laboratory of Marine Ecosystem Dynamics, Second Institute of Oceanography, Ministry of Natural Resources, Hangzhou 310012, China
[7] Institute of Arctic Climate and Environment Research, Japan Agency for Marine-Earth Science and Technology (JAMSTEC), Yokosuka, Japan
[8] NIOZ Royal Netherlands Institute for Sea Research, Department of Ocean Systems (OCS), Texel, the Netherlands
[9] Meteorological Research Institute, Tsukuba, Japan
[10] Global Ocean Observation Research Center, Research Institute for Global Change, Japan Agency for Marine-Earth Science and Technology (JAMSTEC), Yokosuka, Japan
*Corresponding author, email: wcai@udel.edu

Abstract

The Chukchi Sea is an increasing CO_2 sink driven by rapid climate changes. Understanding the seasonal variation of air-sea CO_2 exchange and the underlying mechanisms of biogeochemical dynamics is important for predicting impacts of climate change on and feedbacks by the ocean. Here, we present a unique dataset of underway sea surface partial pressure of CO_2 ($p$$CO_2$) and discrete samples of biogeochemical properties collected in five consecutive cruises in 2014 and examine the seasonal variations in air-sea CO_2 flux and net community production (NCP). We found that thermal and non-thermal effects have different impacts on sea surface $p$$CO_2$ and thus the air-sea CO_2 flux in different water masses. The Bering summer water combined with meltwater has a significantly greater atmospheric CO_2 uptake potential than that of the Alaskan Coastal Water in the southern Chukchi Sea in summer, due to stronger biological CO_2 removal and a weaker thermal effect. By analyzing the seasonal drawdown of dissolved inorganic carbon (DIC) and nutrients, we found that DIC-based NCP was higher than nitrate-based NCP by 66-84% and attributable to partially decoupled C and N uptake because of a variable phytoplankton stoichiometry. A box model with a non-Redfield C:N uptake ratio can adequately reproduce observed $p$$CO_2$ and DIC, which reveals that, during the intensive growing season (late spring to early summer), 30%-46% CO_2 uptake in the Chukchi Sea was supported by a flexible stoichiometry of phytoplankton. These findings have important ramification for forecasting the responses of CO_2 uptake of the Chukchi ecosystem to climate change.

Plain language summary

The Chukchi Sea has been suggested to take more CO_2 from the atmosphere as a result of decreased sea ice coverage and increased inflow of nutrient-rich Pacific Water. In order to better understand the seasonal variations in CO_2 uptake and net community production (NCP) on the Chukchi shelf, we examined the data of sea surface partial pressure of CO_2 and biogeochemical properties collected in five consecutive cruises from spring to fall in 2014. We found that the nutrient-rich Bering Summer Water combined with meltwater has a larger CO_2 uptake potential than that of the nutrient-poor Alaska Coastal Water. In addition, we estimated NCP based on the seasonal drawdown of dissolved inorganic carbon and nutrients, and found that NCP derived from carbon deficit was consistently higher than NCP derived from NO_3^-. We attributed this inconsistency to a high C:N uptake ratio because phytoplankton growth may not always follow the canonical Redfield ratio. With a model simulation, we further quantified that this non-Redfield C:N uptake in phytoplankton enables more efficient carbon-fixation and contributes 30%-46% CO_2 uptake from atmosphere during the intensive growing season in the Chukchi Sea.

Key Points:

- Atmospheric CO_2 uptake potential is larger in the nutrient-rich non-Alaska Coastal Water than the nutrient-poor Alaska Coastal Water
- For the most intensive growing period (spring to early summer), NCP estimation was 66%-84% higher based on DIC than NO_3^-.
- A non-Redfield C:N uptake ratio by phytoplankton enables more efficient DIC-fixation and contributes 30%-46% of CO_2 uptake

1 Introduction

As the first region of the Arctic Ocean to receive water and nutrient inputs from the Pacific Ocean, the Chukchi Sea is a unique ecosystem affecting Arctic biogeochemical cycles, food-web function, and air-sea CO_2 fluxes (Bates et al., 2011; Grebmeier et al., 2015; Tremblay et al., 2015). The high biological productivity and the associated strong CO_2 sink of the Chukchi Sea are primarily sustained by northward flowing, nutrient-rich Pacific Water (Lewis et al., 2020; Ardyna et al., 2020; Ouyang et al., 2020; Tu et al., 2021). Woodgate (2018) reported that the annual mean flow of Pacific Water has increased by ~50% between 1990 and 2015, bringing much more nutrients onto the Chukchi shelf, which has led to higher primary production and CO_2 uptake in recent decades (Arrigo and van Dijken, 2015; Lewis et al., 2020). However, the increase of the annual mean transport of different water masses is not proportional (Woodgate, 2018), which implies that the Chukchi ecosystem may respond differently to the volume increase depending on the different properties of the incoming waters. For example, Lowry et al. (2015) suggested that the summer phytoplankton bloom was sustained by the nutrient-rich winter water and that the persistent biological “hotspot” in the northern Chukchi Sea was driven by the flow and confluence of Pacific winter water rather than the summer Alaska Coastal Water (ACW). This was corroborated by a recent model study (Zheng et al., 2021). Counterintuitively, Strong et al. (2016) found that carbon export was larger in the less-productive ACW than in other more productive water masses. Thus, possible changes of water masses and related changes in water column structure may, in return, affect biogeochemical processes in the Chukchi Sea.

In addition, the seasonal evolution of water masses associated with variations in biological processes plays a key role in controlling nutrients and carbon cycles in the Chukchi Sea. High primary production associated with Pacific Water inflow and sea ice retreats transforms the Chukchi Sea from a nutrient-rich system in spring to a nutrient-limited system in summer (Mills et al., 2015; Zhuang et al., 2020). Such a substantial change in nutrient availability potentially changes the uptake ratio of nutrients and carbon by phytoplankton to form particulate organic matter (POM) and dissolved organic matter (DOM) during primary production and complicates our understanding of the seasonal net community production (NCP) and CO_2 uptake from the atmosphere in the Chukchi Sea (Zheng et al., 2021; Tu et al., 2021). Deviations of C:N uptake stoichiometry from the Redfield ratio have been widely observed over the world’s oceans (Koeve, 2006; Park et al., 2008; Martiny et al., 2013). Several model studies have suggested that non-Redfield stoichiometry of phytoplankton should be taken into account to better project the net primary production, food quality and ocean carbon uptake in response to climate change (Buchanan et al., 2018; Kwiatkowski et al., 2018). However, a variable C:N uptake stoichiometry within a seasonal scale is rarely investigated and it is much less known how a non-Redfield C:N assimilation ratio of phytoplankton may affect NCP and CO_2 uptake in a climate-sensitive region such as the Chukchi Sea.

As the Chukchi Sea is one of the fastest changing regions in the world due to anthropogenic climate changes (Onarheim et al., 2018; Stroeve and Notz, 2018; Meredith and Sommerkorn, 2019; Lewis et al., 2020; Woodgate and Peralta-Ferriz, 2021), it is important to better understand the fundamental drivers, causes, and patterns in seasonal biogeochemical dynamics. Although many efforts have been made to demonstrate the seasonal variation in CO_2 fluxes and biogeochemistry in the Chukchi Sea (Lowry et al., 2015; Zheng et al., 2021; Ardyna and Arrigo, 2020; Ouyang et al., 2021), most of them were based on observations that were either within a single season or over multiple seasons across different years. Given that sea ice conditions in the Chukchi Sea vary from year to year, the timing and magnitude of physical and biological processes change correspondingly, perhaps causing a large uncertainty in deconvoluting the complicated relationship between seasonal air-sea CO_2 flux, NCP, and carbon and nutrient consumption using data collected across different years. Therefore, measurements of biogeochemical properties across multiple periods within a single year provide us a great opportunity to elucidate the links between seasonal evolution of water masses and the associated biogeochemical processes and ecosystem responses, which are essential for forecasting the responses of the Chukchi ecosystem to climate change.

Here, we present a dataset of underway sea surface temperature (SST), salinity (SSS) and sea surface CO_2 partial pressure ($p$$CO_2$) measured in five consecutive cruises in the Chukchi Sea from spring to fall in 2014 (Table 1). We take advantage of this unique dataset to examine both the spatial and seasonal variations in sea surface $p$$CO_2$, and then explore the dominant drivers of seasonal $p$$CO_2$ change along water mass evolution. We also use discrete sample-based biogeochemical properties including DIC, total alkalinity (TA), nutrients (NO_3^- and PO_4^{3-}), dissolved oxygen (DO), and chlorophyll *a* (Chl *a*) from three cruises to identify how seasonal evolution of water masses affect biogeochemical dynamics. In addition, we calculated NCP based on seasonal changes in DIC and nutrients and discussed possible mechanisms for the observed inconsistency in the derived NCP values. Finally, we used a box model to evaluate the impacts of non-Redfield C:N uptake by phytoplankton on seasonal CO_2 uptake in the Chukchi Sea.

2 Method

2.1 Study area and water masses

The water mass properties and circulation in the Chukchi Sea have been extensively studied and presented in many previous works (Gong and Pickart, 2015; Corlett and Pickart, et al., 2017; Stabeno et al., 2018; Pacini et al., 2019; Li et al., 2019; Lin et al., 2019; Pickart et al., 2019). Briefly, three main current branches of Pacific Water flow northward through Bering Strait onto the Chukchi Sea shelf (Fig. 1). On the eastern side, the ACW branch flows along the

Alaskan coast towards Barrow Canyon (known as the Alaskan Coastal Current (ACC) in summer and fall). The central branch flows through Central Channel between Herald Shoal and Hanna Shoal (Weingartner et al., 2005; Woodgate and Aagaard, 2005). The western branch transports Anadyr Water along the Siberian coast towards Herald Canyon (Weingartner et al., 2005). However, there is increasing evidence that the flows are not as rigidly confined to these three separate pathways as was originally thought. For example, a portion of western branch flows eastward to the north of Herald Shoal, where it meets the central branch before joining the eastern branch and exiting the shelf via Barrow Canyon (Fig. 1). It is evident that topographic features such as canyons and shoals greatly affect the shelf circulation.

To focus on the Chukchi shelf, data used for this study were limited from 66ºN to 74ºN to a maximum of 120 m to exclude deep waters from the Canada Basin. We adopted the water mass classification used by several previous studies (Table 2; Gong and Pickart, 2015; Corlett and Pickart, et al., 2017; Pickart, et al., 2019; Pacini et al., 2019, Wang et al., 2022). The coldest water is known as Newly-Ventilated Winter Water (NVWW; $T < -1.6$ ℃), which is typically observed from spring to early-summer over the entire shelf. As summer progresses, this winter water can be converted to Remnant Winter Water (RWW; -1.6 ℃ $< T < 0$ ℃) by solar heating or mixing with warmer summer water, which sometimes lasts into summer (Gong and Pickart, 2015). During summer and early fall, the Chukchi Sea mainly contains two Pacific summer waters. The first is ACW, which originates in the Gulf of Alaska. In the summer, the ACC carries predominantly ACW in the eastern Chukchi Sea, in which the water temperature can reach >10 ℃. The second is a combination of Anadyr Water and central Bering Shelf water, which is referred to as Bering Summer Water (BSW). The seasonal sea ice Melt Water (MW) forms a layer of fresh water on the Chukchi shelf. Sometimes it can also be divided into early-season melt water and late-season melt water (Table 2; Gong and Pickart, 2015; Pickart, et al., 2019). This freshwater layer evidently occupies a large portion of the Chukchi/Beaufort shelfbreak regions in the mid- to late-summer. In these regions, the densest and saltiest water, the Atlantic Water (AW; $T > -1.0$ ℃ and $S > 33.6$), can be observed at depths below ~150 m, but it is rarely observed on the Chukchi shelf. However, AW can be upwelled occasionally through Barrow Canyon (Pisareva et al., 2019) and Herald Canyon (Pickart et al., 2010).

2.2 Underway measurements

It is unusual that there are five survey cruises in one year (2014) with underway sea surface temperature (SST), salinity (SSS) and $p\mathrm{CO}_2$ measured in the Chukchi Sea (Table 1). To our knowledge, this is the only year so far with such high-density observations. The underway data were obtained from the SOCAT database (v2020; Bakker et al., 2016) and Japan Agency for Marine-Earth Science and Technology (JAMSTEC) (Table 1). Specifically, the underway SST and SSS were measured using an underway water monitoring system in an intake port near the bow of the ships (5-7 m below the waterline). The underway sea surface $p\mathrm{CO}_2$ from USCGC Healy and RV Xuelong was measured using an underway $p\mathrm{CO}_2$ system (General Oceanic, USA) described in Pierrot et al. (2009). The data from RV Mirai was analyzed by a Greenhouse Gas Analyzer (Los Gatos Research, USA). These systems were monitored and calibrated with four certified gas standards (NOAA) every 2-3 hours. The overall precision of the reported sea surface $p\mathrm{CO}_2$ values was estimated to be ± 2 μatm. The underway $p\mathrm{CO}_2$ system and data reduction procedure were described by Pierrot et al. (2009).

2.3 Discrete sample analysis

Discrete biogeochemical samples were collected during three cruises (Table 1). The datasets of discrete samples included nutrients ($\mathrm{NO_3^-}$ and $\mathrm{PO_4^{3-}}$), dissolved oxygen (DO), Chl *a*, DIC and TA. The data, collected from USCGC Healy in spring, from RV Xuelong in summer, and from RV Mirai in fall, have been archived in publicly accessible data centers (Table 1).

In the spring cruise, nutrients, DO and Chl *a* were measured onboard. Nutrient samples were determined using a Seal Analytical continuous-flow AutoAnalyzer 3 following a modified procedure after Armstrong et al. (1967). DO was measured using a spectrophotometer following the standard Winkler titration method, with a precision of ±1 μmol $\mathrm{kg^{-1}}$. Chl *a* measurements were made using a Turner 10-AU fluorometer (Turner Designs, Inc.) (Holm-Hansen et al. 1965) and were calibrated against a pure Chl *a* standard (Sigma). See more description of sampling and analysis of nutrients, DO, and Chl *a* in Arrigo et al. (2017). DIC and TA samples were collected into 250 mL borosilicate glass bottles poisoned with 100 μL saturated $\mathrm{HgCl_2}$ solution to prevent biological activity following the procedure described in Dickson et al. (2007). DIC and TA samples were analyzed at the University of Southampton, UK via coulometric (DIC) and potentiometric (TA) titration methods using a VINDTA 3C (Marianda), with a precision of ± 2 μmol kg^{-1}.

In the summer cruise, nutrient data were measured onboard using a San^{++} automated continuous flow autoanalyzer with a precision of ±2% (SKALAR Inc., Netherlands). The detection limits were 0.1 μM for NO_3^- and 0.03 μM for PO_4^{3-}. Chl *a* samples were measured following similar procedures to the spring expedition. DO was measured onboard using the spectrophotometric method based on Winkler titration with a precision of ±1 μmol kg^{-1}. See more descriptions of sampling and analysis of nutrients and Chl *a* samples in Zhuang et al. (2020). DIC and TA samples were collected following similar procedures described above, and then were analyzed at the University of Delaware, USA. DIC samples were analyzed using a LiCOR LI 7000 infrared CO_2 detector coupled to an automated DIC analyzer (Apollo SciTech, USA). TA samples were measured via open-cell potentiometric titration system (Apollo SciTech, USA). The precision of the DIC and TA measurements was ~0.1% (~± 2 μmol kg^{-}1; Chen et al., 2015).

In the fall cruise, nutrients were analyzed using QuAAtro system. DO was measured via the spectrophotometric Winkler titration method (Kimoto Electric Co. LTD) following the World Ocean Circulation Experiment Hydrographic Program method (Dickson, 1996). The precision of DO measurement was 0.23 μmol kg^{-1} (Kimoto Electric Co. LTD). Chl *a* was measured using a fluorophotometer (Turner Designs) (Welschmeyer et al. 1994). Nutrient samples were analyzed following the GO-SHIP Repeat Hydrography Manual (Hydes et al., 2010) using reference materials for nutrients in seawater (Sato et al., 2010). The precision was 0.08% for NO_3^- and 0.14% for PO_4^{3-}. See more descriptions of sampling and analysis of nutrient, DO, and Chl *a* in Nishino et al. (2020). DIC was measured using an automated coulometric analyzer (Nippon ANS, Inc.) with a precision of ± 0.7 μmol kg^{-1} and TA samples were measured using a custom spectrophotometric system (Nippon ANS, Inc.) with a precision of ±0.57 μmol kg^{-1}. Note that DIC and TA samples collected in all three cruises were calibrated using certified reference materials (CRMs) from Scripps Institution of Oceanography.

In addition, discrete pCO$_2$ was calculated with surface TA and DIC (<10 m) to increase the data coverage over temporal and spatial scales. The pCO$_2$ was calculated by the seacarb package in R (Gattuso et al., 2018) with carbonate dissociation constants of Millero et al. (2006), as recommended by Evans et al. (2015). The uncertainty of pCO_2 values computed from TA and DIC is estimated to be ±18 μatm (RMSE) with a mean systematic difference from the observed pCO_2 of 0.5 μatm (N=111).

2.4 Decomposition of seasonal pCO_2 change

To explore the dominant drivers for seasonal pCO_2 change in each water mass, we decomposed the net change of pCO_2 into thermal and non-thermal effects, assuming that these two effects altered pCO_2 within a time frame much shorter than the residence time of the water mass on the Chukchi shelf. Therefore, the net change in pCO_2 ($\Delta(pCO_2)$) could be calculated as the difference between the initial pCO_2 (pCO_{2ini}) under the ice in spring (538 ± 68 µatm) and the observed pCO_2 (pCO_{2ob}) at a given sampling time:

$$\Delta(pCO_2) = pCO_{2ob} - pCO_{2ini} \qquad (1).$$

The potential thermal effect on pCO_2 change ($\Delta(pCO_2)_T$) was driven by the seasonal variation in SST and was quantified by adjusting the initial pCO_2 to the observed temperature (Takahashi et al., 1993):

$$\Delta(pCO_2)_T = pCO_{2ini} \times \exp(0.0423 \times (T_{obs} - T_{spring})) - pCO_{2ini} \qquad (2)$$

where T_{obs} is the observed temperature and T_{spring} is the mean temperature observed under the ice in spring (-1.60 ºC). The non-thermal effect on pCO_2 change ($\Delta(pCO_2)_{nT}$) was mainly driven by the seasonal biological CO_2 drawdown and ice melt, and was calculated as the difference between the observed total net seasonal change and the thermal effect:

$$\Delta(pCO_2)_{nT} = \Delta(pCO_2) - \Delta(pCO_2)_T\ . \qquad (3).$$

2.5 Seasonal CO_2 flux calculation

To avoid calculational bias induced by the overweighted impact of highly dense data point concentrated within a small area, we averaged the data points into daily-grids of 0.25° latitude × 0.25° longitude, and then we calculated seasonal air-sea CO_2 flux for each grid following:

$$FCO_2 = K_s \cdot k_{CO2} \cdot \Delta pCO_2 \qquad (4)$$

where K_s is the solubility of CO_2 and k_{CO2} is the CO_2 gas transfer velocity. K_s was calculated using underway SST and SSS (Weiss, 1974). The value of k_{CO2} (cm/hr) is estimated from the second moment of wind speed at 10 m above the sea surface, $<U_{10}^2>$ (Wanninkhof 2014):

$$k_{CO2} = 0.251 \cdot <U_{10}^2> \cdot (Sc/660)^{-0.5} \cdot (1 - \frac{ice\%}{100}) \qquad (5).$$

To calculate $<U_{10}^2>$, we used the wind product from the NCEP-DOE Reanalysis 2 dataset (https://www.esrl.noaa.gov/psd/data/gridded/data.ncep.reanalysis2.html). A regional mean of $<U_{10}^2>$ over the study period was derived from the 6-hour wind speed squared. The term ice% is the sea ice concentration, which is averaged from daily ice% data obtained from the Scanning Multichannel Microwave Radiometer (SMMR) on the Nimbus-7 satellite and the Special Sensor Microwave/Imager (SSM/I) sensors on the Defense Meteorological Satellite Program's (DMSP)-F8, -F11, and -F13 satellites (https://nsidc.org/data/nsidc-0079; Comiso, 2017). For the area with heavy ice covered, we adopted Takahashi et al., (2009) approach that for sea ice where satellite observation is >90% ice cover, a 10% open water area is assumed. In this way, 10% of the open water persisted for CO_2 flux in the area with >90% ice cover where satellite data with resolution of 25 km × 25 km fails to resolve fine scale structure, such as leads.

The air-sea CO_2 gradient (ΔpCO_2) is calculated as:

$$\Delta pCO_2 = pCO_2^{sea} - pCO_2^{air} \qquad (6)$$

where the pCO_2^{sea} is from underway observations and the pCO_2^{air} is derived from monthly average atmospheric CO_2 concentrations in dry air (xCO_2 (ppm)) measured at Point Barrow, Alaska (https://www.esrl.noaa.gov/gmd/dv/data/index.php?parameter_name=Carbon%2BDioxide&frequency=Monthly%2BAverages&site=BRW; Thoning et al., 2021). Then xCO_2 is corrected for water vapor pressure content to pCO_2^{air}:

$$pCO_2^{air} = xCO_2 \cdot (Psl - Pw) \qquad (7)$$

where Psl is sea level pressure and Pw is water vapor pressure. Regional mean Psl over the study period was averaged from a satellite reanalysis product (NCEP-DOE Reanalysis 2, https://www.esrl.noaa.gov/psd/data/gridded/data.ncep.reanalysis2.html). Pw was calculated from Psl and SST (Buck, 1981).

2.6 Estimates of net community production

The NCP can be estimated from the nutrient and DIC changes in the upper mixed layer. Since the residence time of water masses on the Chukchi Sea shelf (3 - 7.5 months) (Stabeno et al., 2018; Woodgate and Peralta-Ferriz, 2021) is longer than the timespan of a phytoplankton bloom (< 1-2 months), we can assume that water masses move as a single parcel over the shelf, where physical (mostly warming and freshening) and biogeochemical changes occur over time. Therefore, at any particular location, the observed drawdown of nutrients and DIC in the surface mixed layer can be attributed to NCP. However, nutrient and DIC concentrations are not only influenced by NCP, but also by meltwater/river-runoff dilution, and in the case of DIC, by air-sea CO_2 exchange and $CaCO_3$ dissolution and formation. Thus, to quantify the biological-induced changes in nutrients, DIC, and TA, we normalized all nutrient (NO_3^- and PO_4^{3-}), DIC and TA concentrations to a reference salinity (S_0, i.e., mean salinity under the ice in spring) to remove the impact of Arctic Ocean freshwater input into the Pacific winter water. As river discharge impact in spring and early summer is either limited to the estuarine and nearshore areas within the Arctic or treated as part of the Pacific water endmember (Text S1 and Fig. S1), the salinity change in Chukchi Sea is mainly attributed to ice melt dilution for period of interest (spring to early summer); thus, non-zero meltwater endmembers are used (Friis et al., 2003; Jiang et al. 2008):

$$\mathrm{nDIC} = \frac{\mathrm{DIC} - \mathrm{DIC}_{S=0}}{S} \times S_0 + \mathrm{DIC}_{S=0} \qquad (8)$$

$$\mathrm{nTA} = \frac{\mathrm{TA} - \mathrm{TA}_{S=0}}{S} \times S_0 + \mathrm{TA}_{S=0} \qquad (9)$$

$$\mathrm{nNO_3^-} = \frac{\mathrm{NO_3^-} - \mathrm{NO_3^-}_{\,S=0}}{S} \times S_0 + \mathrm{NO_3^-}_{\,S=0} \qquad (10)$$

The meltwater salinity, DIC and TA values are set as 5, 400 μmol kg^{-1}, 460 μmol kg^{-1} (Rysgaard et al., 2007), respectively, which are equivalent to $DIC_{S=0}$ = 60 μmol kg^{-1} and $TA_{S=0}$ = 106 μmol kg^{-1} (Cai et al., 2010; Ouyang et al., 2020). The contributions of meltwater to NO_3^- (μM) and PO_4^{3-} (μM) concentrations are negligible (Clark et al., 2020).

The deficit of nNO_3^- (or nPO_4^{3-}) is the result of phytoplankton uptake between the time before the phytoplankton bloom begins (t_1) in spring and the time of sampling (t_2). Then, the vertical integral of the deficit of nNO_3^- (or nPO_4^{3-}) within surface mixed layer is assumed to be equal to NCP at any given location over the time interval between t_1 and t_2 (Δt),

$$NCP_{N\text{-based}} = (nNO^-_{3\,t1} - nNO^-_{3\,t2}) \times MLD / \Delta t \qquad (11)$$

Analogue equations of (9) and (10) can be written for nPO_4^{3-}. The average mixed layer depth (MLD) of 25 m was used in this study. While this is a highly simplified treatment, the MLD uncertainty would apply equally to C-, N-, and P-based NCP. The estimates of nutrient-based NCP were then converted to carbon units by multiplying by a molar C:N:P uptake ratio of 106:16:1 (Redfield 1958; Hansell et al., 1993; Codispoti et al., 2013; Arrigo et al., 2017).

The nDIC change reflects the influence of both phytoplankton uptake, air-sea CO_2 exchange, and $CaCO_3$ dissolution and formation. Therefore, we calculated biological-induced nDIC change by subtracting the DIC added by the CO_2 influx and possible $CaCO_3$ formation and dissolution ($CaCO_3 + H_2O + CO_2 \leftrightarrow Ca^{2+} + 2HCO_3^-$):

$$NCP_{DIC\text{-based}} = (nDIC_{t1} \times \rho_{t1} - nDIC_{t2} \times \rho_{t2} - \Delta DIC_{CaCO3}) \times MLD / \Delta t - CO_2\ flux \qquad (12)$$

where ρ is the water density and CO_2 flux term was calculated following equation (4). The term of ΔDIC_{CaCO3} can be quantified as half of the change in salinity-normalized TA (nTA) corrected for the removal of NO_3^- to form organic matter (Brewer and Goldman, 1976; Lee 2001):

$$\Delta DIC_{CaCO3} = (\Delta nTA \times \rho - \Delta NO_3^-) \times 0.5 \qquad (13)$$

Note that due to lack of information we are not able to differentiate biological calcification and the dissolution of $CaCO_3$ mineral (ikaite) trapped in the melting ice.

2.6 Box model

The goal of the box model is to investigate how a flexible C:N uptake ratio by phytoplankton affects DIC fixation and air-sea CO_2 fluxes in the Chukchi Sea. Similar box model approaches have been described in previous studies (Ouyang et al., 2020; Ouyang et al., 2021). Briefly, the initial TA and DIC values were set to the mean value of observations in the surface mixed layer in late spring, and the initial sea surface pCO_2 was calculated from the initial TA and DIC using the seacarb package in R (Gattuso et al., 2018). TA in the subsequent season was linearly interpolated based on observations. For each simulation step, sea surface pCO_2 was calculated from TA and DIC at the corresponding step. The change in DIC inventory (ΔDIC) in the surface mixed layer was calculated as

$$\Delta DIC_t = (FCO_{2t} + NCP_t) \times \tau / (MLD \times \rho) + \Delta DIC_{(diluted)t} \qquad (14)$$

where FCO_{2t}, NCP_t, and $\Delta DIC_{(diluted)t}$ indicate the changes in DIC inventory in the mixed layer induced by the CO_2 air-sea flux, NCP, and dilution by meltwater at simulation time step t, respectively. In this case, the simulation time interval (τ) is 1 day. The surface seawater density, ρ, was calculated using SST and SSS. The FCO_2 term was calculated with equation (4). The $\Delta DIC_{(diluted)t}$ term was computed by simplifying the ice melt dilution and assuming that the ratio of TA/DIC in the thin first-year ice nearly equals that in the surface seawater (Rysgaard et al., 2007). Thus,

$$\Delta DIC_{(diluted)t} = (TA_{t+1} - TA_t) / TA_t \times DIC_t \qquad (15).$$

Because the Chukchi Sea is N-limited during the growing season (Mills et al., 2015; 2018), NCP_t was calculated based on nitrate; $NCP_{N\text{-}based}$. Two scenarios with different C:N uptake ratios were examined in the box model. For the fixed-stoichiometry scenario, a C:N uptake ratio of 6.6 (Redfield ratio) was used. For the non-Redfield scenario, much higher C:N uptake ratios were used (i.e., 10.9 and 12.1 in Table 5). Therefore,

$$NCP_t = NCP_{N\text{-}based} \times C\text{:}N \text{ ratio} \qquad (16)$$

and DIC at time step t+1 was iteratively calculated as follows:

$$DIC_{t+1} = DIC_t + \Delta DIC_t \qquad (17).$$

With the new DIC and TA, a new pCO$_2$ was calculated for the next simulation step, and this simulation process repeated until the last day of the simulation.

3 Results

3.1 Sea surface temperature, salinity, and pCO$_2$

Underway SST, SSS, and pCO$_2$ were measured during five cruises in the Chukchi Sea, from May through September in 2014, providing a consistent way to examine the seasonal transition of the ocean from a CO$_2$ source to a sink and to explore the role of changing water masses.

Because sea ice melt began in the southern portion of the Chukchi Sea in early June, we divided the spring observations into two periods: early spring (May 15 – May 31) and late spring (June 1 – June 21). Clearly, SST distribution was greatly affected by sea ice (Fig. 2 a). SST was near freezing (-1.67 ± 0.07 ℃) under the ice in the north, while SST in the south was slightly warmer (-1.28 ± 0.28℃). The location of SST fronts corresponded well with the edge of heavy ice cover around 69.5ºN (ice concentration ~80%). However, the distribution of SSS was not as closely correlated with ice as SST was (Fig. 2 b). In the southern portion of Chukchi Sea, the surface water was relatively fresher due to mixing with newly melted water and river discharge. The saltier water appeared in the eastern and central Chukchi Sea under the ice. Interestingly, relatively warmer and fresher water was also found in the northeast part of Chukchi Sea towards the shelfbreak (Fig. 2 a-b), which was likely due to local ice melt events. The average pCO$_2$ in the south was 309 ± 50 µatm, which was much lower than that in the north (536 ± 74 µatm). Such a contrasting pattern in pCO$_2$ indicated that the southern ice-free Chukchi Sea had already become a CO$_2$ sink while the northern ice-covered Chukchi Sea still remained supersaturated with respect to atmospheric CO$_2$ (~400 µatm) and was a potentially strong CO$_2$ source in early spring (Fig. 2 c).

As sea ice retreated northwards in the late spring (Fig. 2 d-f), more warm and fresh waters advected from south to north. However, their impacts were confined by sea ice. The SST, SSS, and $p\mathrm{CO_2}$ values in the ice-covered area were similar to those earlier in the spring. Only a few observations south of the ice edge showed signals of warmer and fresher Pacific summer waters. Although there were no observations in the southern Chukchi Sea during this period, we expect that water there might have become warmer and fresher with much lower $p\mathrm{CO_2}$ compared to early spring, which was confirmed by observations on the last day (June 21) of the spring cruise in the south of Bering Strait (Fig. 2 d-f).

In early summer (July 9 – August 7), the ice edge retreated further northwards to around 71-72ºN (Fig. 3 a-f). The mean SST increased to 6.64 ± 1.22 ℃ in the southern and central Chukchi Sea but remained low (-0.83 ± 1.31 ℃) under the ice in the northern Chukchi Sea (Fig. 3 a and d). The distribution of SSS was not only affected by the northward advection of water but also by dilution by meltwater. Compared to spring, the mean SSS (31.0 ± 0.7) over much of the southern and central Chukchi Sea had decreased by 0.5-1.0, although this decrease was more substantial (by 3-4) near the shelfbreak (Fig. 3 b and e). The most notable change in the carbonate system between spring and early summer was a widespread reduction in sea surface $p\mathrm{CO_2}$. The lowest $p\mathrm{CO_2}$ values were found in the vicinity of the Bering Strait in the south and along the ice edge in the northern Chukchi Sea (Fig. 3 c and f).

The Chukchi Sea had become a completely ice-free region in late summer (August 12 – September 9; Fig. 3 g-l). SST continued to increase over the entire Chukchi shelf (Fig. 3 g and j). The highest SST appeared in the middle of August along the Alaska coast, reaching up to ~11 ℃ (Fig. 3 g). The SSS showed a similar distribution as in early summer, with saltier water in the southern and central Chukchi Sea and fresher water in the eastern and northern portion as a result of massive sea-ice melt and river discharge (Fig. 3 h and k). Compared to early summer, the mean sea surface $p\mathrm{CO_2}$ in late summer increased from 202 ± 63 μatm to 265 ± 69 μatm but remained much lower than the atmospheric $p\mathrm{CO_2}$ (Fig. 3 i and l). It is noteworthy that the lowest $p\mathrm{CO_2}$ was observed repeatedly north of Bering Strait and in the area surrounding Hanna Shoal (Fig. 3 i and l).

Between late summer and fall, the mean SST over the entire shelf decreased from 5.42 ± 3.04 ℃ to 3.49 ± 1.73 ℃, while the mean SSS remained nearly unchanged (Fig. 4 a-b). For most of the Chukchi Sea, surface water $p\mathrm{CO_2}$ was lower than the atmospheric $p\mathrm{CO_2}$, averaging 283 ±

50 µatm, indicating that the CO_2 sink lasted into fall. However, extremely high pCO_2 started to appear in the northern Bering Sea along the western pathway of Pacific Summer Water (Fig. 4 c).

3.2 Water column structure

Discrete samples of biogeochemical parameters were collected during three cruises (Table 1). Since these three cruises conducted survey sections along the Central Channel, we are able to show the seasonal evolution of biogeochemical properties in the water column along a transect from the Bering Strait extending to the shelf break in the northern Chukchi Sea.

In early spring, water columns on the Chukchi shelf were well mixed, exhibiting little vertical structure for most biogeochemical properties (Fig. 5). The exceptions were a subsurface (20-30 m) Chl *a* maximum in the southern Chukchi Sea (Fig. 5 g) and the frontal structures of large gradient in DIC and NO_3^- across the shelf breaks (73ºN; Fig. 5 f and h). However, latitudinal patterns were significantly different from the south to the north, which was due to different levels of primary production regulated by the timing of ice melting. Seawater temperature and salinity under the ice were within a narrow range of -1.78 ℃ to -1.60℃ and 32 to 33, respectively, indicating that during this period, almost all waters on the northern shelf were NVWW (Fig. 5 d). Low concentrations of Chl *a* (<1 µg l^{-1}), high NO_3^- (>15 µM), and positive apparent oxygen utilization (AOU) beneath the ice suggested that the spring bloom had not yet started there (Fig. 5 g-i) and the ambient high DIC was likely accumulated from remineralization in the previous winter water (Fig. 5 f). In contrast, primary production within RWW had begun in the southern Chukchi Sea, indicated by a much higher Chl *a* concentration (>4 µg l^{-1}), lower NO_3^-, and negative AOU (Fig. 5 g-i). As a result, mean DIC in the south was ~100 µmol kg^{-1} lower than that in the north (Fig. 5 f, Table 3).

A few weeks later, as the ice conditions changed, the water at the ice edge became warmer and fresher as a result of local sea ice melt freshening together with atmospheric heating (70.5ºN; Fig. 6 a-b). Although most water columns still consisted of NVWW and were well mixed, a two-layer structure appeared in the southernmost stations (Fig. 6 c), indicating that seasonal stratification of the water column had begun. In addition, the Chl *a* concentration increased to 2.8±2.2 µg l^{-1} and the previously positive AOU had turned negative, indicating net oxygen production by a phytoplankton bloom (Fig. 6 i). The late-spring ice retreat further strengthened primary production in the northern Chukchi Sea. In turn, the associated biological CO_2 drawdown resulted in lower DIC in the surface layer (Fig. 6 f).

Conditions during the early summer transect were vastly different from the spring conditions (Fig. 7). The fully mixed water column representative of spring conditions had transformed into a clear two-layer structure with a shallow, warm and fresh surface mixed layer with ACW properties separated by a halocline from BSW and winter water near the bottom (Fig. 7 a-d). Strong primary production over the shelf led to a large reduction in DIC and NO_3^- in the surface mixed layer (Fig. 7 f and h; Table 3). Simultaneously, the surface extremely high O_2 (AOU < -100 μmol kg^{-1}) coincided with the subsurface Chl *a* maximum in the north of Bering Strait and over the shelfbreak (Fig. 7 g and i). Interestingly, the surface extremely low NO_3^- (<1 μM) and supersaturated DO extended throughout the water column in the central Chukchi Sea (68ºN -70ºN Fig. 7 g-h), which were likely induced by local mixing events occasionally breaking the two-layer structure or a mechanical overturning induced by internal wave mixing (Kawaguchi et al., 2015; Nishino et al., 2015).

Although we only have observations in the southern Chukchi Sea and in the Canada Basin (i.e., no data in the central and northern shelf) in late summer, it is likely that the strong two-layer stratification remained in the water column over most of the Chukchi Sea (Fig. 8). The highest Chl *a* concentration (> 25 μg l^{-1}) repeatedly appeared at the similar location in the north of Bering Strait associated with BSW (68ºN; Fig. 8 d and g) but AOU increased from <-100 to ~ -30 μmol kg^{-1} (Fig. 8 i). The surface DIC in the southern Chukchi Sea (probably in the northern Chukchi Sea as well) became higher than in early summer by ~100 μmol kg^{-1} (Fig. 8 f). As the water column stratification strengthened, the gradients in DIC, NO_3^- and AOU between surface and bottom layers became larger (Fig. 8 f, h, i; Table 3). The highest NO_3^- (>20 μM) was observed in the bottom waters in the southern Chukchi Sea.

Three weeks later in fall, the stratified vertical structure persisted over most of the shelf area (Fig. 9 a-d). However, a widespread reduction in Chl a concentrations suggested that primary production had become much weaker. High Chl a concentrations were only observed in the biological hot spot in the southern Chukchi Sea (68ºN; Fig. 9 g), which was present throughout the entire growing season. NO_3^- became depleted in the surface waters (Fig. 9 h), limiting further phytoplankton growth, while replenishment of NO_3^- was observed in bottom waters in the southern Chukchi Sea. Consequently, surface O_2 approached equilibrium with the atmosphere (AOU was ~0 μmol kg^{-1}) and surface DIC remained the same as it was in late summer (Fig. 9 f and i).

4 Discussion

4.1 Water mass evolution and CO_2 flux

Seasonal evolution of water masses affects primary production and subsequently air-sea CO_2 exchange. To investigate the correlation between water mass change and ocean CO_2 uptake, we first illustrate the relationship between water mass properties and seasonal change in sea surface pCO_2 in T/S diagrams (Fig. 10). In spring, most of the net change in pCO_2 was negative since a high pCO_2 value (i.e., 538 μatm) in the earlier winter water under the ice was used as the reference value (Fig. 10 a). The high pCO_2 values that exceeded atmospheric pCO_2 were concentrated within the cold and salty NVWW and RWW beneath the ice, which was resulted from remineralization in and vertical mixing of waters from the previous winter (Fig. 10 a). As sea ice started to retreat in late spring and early summer, the dilution by meltwater and strong biological CO_2 uptake led to extremely low (<100 μatm) pCO_2 along the ice edge (Fig. 3 c and f) with the largest seasonal reduction in the early-season meltwater (Early-MW; Fig. 10 b). These two processes primarily triggered the transition from a CO_2 source to a sink within a few weeks. During this period, the average CO_2 flux changed from 1.1 ± 1.1 mmol m^{-2} d^{-1} (from sea to air, or a source) to -7.2 ± 3.4 mmol m^{-2} d^{-1} (from air to sea, or a sink) in the northern Chukchi Sea (Fig. 11 a and b; Table 4). As the season progressed, the surface NVWW and RWW were largely transformed or replaced by summer Pacific waters (i.e., ACW and BSW). Consequently, the nutrient-rich BSW sustained strong primary production and resulted in another extremely strong CO_2 uptake center in the southern Chukchi Sea north of the Bering Strait (~ 68ºN, Fig. 11 c), whereas the warmer (SST >8 ºC), relatively nutrient-poor ACW had relatively weaker CO_2 uptake along the eastern coastal area (Fig. 11 c). We noticed a small area of CO_2 efflux in the eastern Chukchi Sea in late summer (Fig.11 c) and an area of CO_2 source water in the BSW regime in the southern Chukchi Sea in fall (~69ºN; Fig. 11 d). These high pCO_2 surface waters were likely due to local vertical mixing as energetic currents in this area of shallow depths (< 50 m) could break down stratified vertical structure and bring high pCO_2 bottom water up to the surface (Brown et al., 2015). The regional mean CO_2 flux in late summer and fall were estimated to range from -18.3±8.9 to -10.5±8.4 mmol m^{-2} d^{-1} in the southern Chukchi Sea and from -13.3±6.6 to -21.1±2.9 in the northern Chukchi Sea (Table 4).

Decomposition of the seasonal change in pCO_2 provides more insight into the controlling drivers. Between spring and early summer, the largest reduction in pCO_2 was observed in the early-season MW and BSW, while the pCO_2 reduction in the ACW was relatively less (Fig. 10 b). Specifically, the warm ACW and river runoff have the largest thermal effect on changing pCO_2; a warming of more than 10ºC in SST along could potentially increase pCO_2 by ~300 µatm (Fig. 10 f). In contrast, thermal effects were the relatively weaker driver for pCO_2 change in both the BSW and MW (Fig. 10 f). In addition, the nutrient-rich BSW provided a continued nutrient supply for sustaining primary production and biological CO_2 drawdown along the Central Channel pathway. The strong reduction of pCO_2 within BSW and MW domains (Fig. 10 j) even exceeded the increase induced by warming (Fig. 10 f), resulting in a net decrease in pCO_2 and a strong CO_2 sink (Fig. 10 b and Fig. 11 b). Similar patterns existed in the following seasons (Fig. 10 and Fig. 11 c and d)

As the CO_2 uptake mainly occurred within Pacific Summer Water and thermal and non-thermal effects had different impacts on CO_2 flux in different water masses, we estimated CO_2 fluxes separately in two types of water masses: the ACW (including RW) and non-ACW (including BSW and MW but excluding NVWW and RWW). We found that the CO_2 uptake potential in the nutrient-rich non-ACW was significantly larger than that in the relatively nutrient-poor ACW in the southern Chukchi Sea during summer months (Table 4). Such difference became less contrasting because these two water masses tended to have more similarities as they were modified by mixing, meltwater input, and other local processes in the northern Chukchi Sea (Table 4). This finding has important implications for CO_2 uptake in the Chukchi Sea. Woodgate (2018) found that annual inflow of Pacific waters has increased by more than 50% from 1990 to 2015, but there was no significant trend in annual mean flow in the ACC. Corlett and Pickart (2017) also confirmed that BSW (non-ACW) increased relative to ACW on the Chukchi slope from 2002-2004 to 2009-2014. Thus, non-ACW was likely responsible for the increase in total annual flow. If this is confirmed to be the case, we suggest that the Chukchi Sea will be a greater CO_2 sink in the future, as non-ACW will play a bigger role in CO_2 uptake.

4.2 Water mass evolution and net community production

Spatial and temporal variations in water mass distributions substantially affect primary production in the Chukchi Sea during the growing season. In spring, both the southern and northern Chukchi Sea were largely occupied by the winter water (NVWW and RWW), which provided sufficient nutrients for phytoplankton to bloom (Fig. 12 a-d; Arrigo et al., 2017). From late spring to early summer, winter waters were gradually transformed to or replaced by the warmer summer waters (BSW and ACW), particularly in the surface layer (Fig. 12). At the same time, both normalized nitrate ($\mathrm{nNO_3^-}$), phosphate ($\mathrm{nPO_4^{3-}}$), and DIC (nDIC) decreased rapidly as a result of strong consumption due to phytoplankton growth. In late summer and fall, only a small portion of RWW existed in the bottom layer in the northern Chukchi Sea, while BSW and ACW accounted for the majority of surface water over the entire Chukchi Sea (Fig. 12). For the bottom layer, $\mathrm{NO_3^-}$ and $\mathrm{PO_4^{3-}}$ were replenished by a combination of advection of nutrient-rich BSW and possible vertical mixing from the bottom layer. This input of $\mathrm{NO_3^-}$ and $\mathrm{PO_4^{3-}}$ exceeded the biological drawdown in the southern Chukchi Sea, which resulted in a net increase in $\mathrm{nNO_3^-}$ and $\mathrm{nPO_4^{3-}}$ concentrations in both the surface and bottom layers (Fig. 12 a and c). However, in the northern Chukchi Sea, $\mathrm{nNO_3^-}$ concentration remained depleted and $\mathrm{nPO_4^{3-}}$ was the same in the surface layer but both increased in the bottom waters (Fig. 11 b and d). The high residual $\mathrm{nNO_3^-}$ and $\mathrm{nPO_4^{3-}}$ in the bottom water were likely the remaining within winter waters rather than BSW delivery (Zheng et al., 2021).

As primary production is the main driver modifying water column biogeochemical properties during the growing season, we estimated NCP using the observed drawdown of nutrients ($\mathrm{nNO_3^-}$ and $\mathrm{nPO_4^{3-}}$) and nDIC in the surface mixed layer. The spring concentrations of $\mathrm{nNO_3^-}$, $\mathrm{nPO_4^{3-}}$and nDIC were used as an initial condition to determine the subsequent biological drawdown by NCP. As the largest changes were observed in the period between spring and early summer, which were also associated with the most evident water mass evolution, therefore, we will mainly focus on this period in the following discussion.

Although there were no observations in late spring in the southern Chukchi Sea (Fig. 12 a, c, and e), a water mass analysis showing that the winter water still made up most of the southern Chukchi Sea during this period (Pacini et al., 2019). Based on that, we assume that water parcel in the southern Chukchi Sea between early spring and early summer was not greatly changed and it is still appropriate to estimate NCP based on the deficits of nutrients and nDIC. The decreases of nDIC in the surface mixed layer between spring and early summer were 79±87 and 95±51 μmol kg^{-1}, respectively, in the southern and northern Chukchi Sea (Fig. 12 e and f; Table 5). After correcting for air-sea gas exchange and $CaCO_3$ formation and dissolution, these nDIC deficits yield mean NCP estimates of 38.4 ± 26.2 and 61.4 ± 20.0 mmol C m^{-2} d^{-1}, respectively, in the southern and northern Chukchi Sea (Table 5). Our nDIC-based NCP estimates in 2014 were comparable with NCP estimates made using a similar approach in early summer in 2004 in the northern Chukchi Sea (Mathis et al., 2009). During the same period, nNO_3^- in the surface mixed layer was fully depleted over the entire Chukchi Sea (Fig. 12 a and b). Such NO_3^- depletion was also observed in early summer in 2010 and 2011 (Lowry et al., 2015; Brown et al., 2015). The mean nNO_3^- deficits in 2014 were 10.24 ± 0.20 and 9.92 ±1.57 μM in the southern and northern Chukchi Sea, respectively (Table 5), giving an NCP of 3.51± 0.07 and 5.06 ± 0.80 mmol N m^{-2} d^{-1} in the southern and northern Chukchi Sea, respectively (Table 5). Because the mean nPO_4^{3-} deficits were 1.19±0.11 and 0.94±0.21 μM in the southern and northern Chukchi Sea, respectively (Table 5), nPO_4^{3-}-based NCP was estimated to be 0.41±0.04 and 0.48 ± 0.11 mmol P m^{-2} d^{-1} in the southern and northern Chukchi Sea, respectively (Table 5). Given a molar C:N:P uptake ratio of 106:16:1 (Redfield 1958), nNO_3^--based NCP was estimated to be 23.2 ± 0.5 and 33.4 ± 5.3 mmol C m^{-2} d^{-1} in the southern and northern Chukchi Sea. The analogous rates for nPO_4^{3-}-based NCP were 43.3 ± 4.0 and 50.9 ± 11.3 mmol C m^{-2} d^{-1}, respectively. Thus, the nDIC-based NCP was significantly higher than the NCP derived from nNO_3^- consumption by 66-84% and was close to or slightly higher than nPO_4^{3-}-based NCP (Table 5). Although river off or precipitation may dominate endmembers in some locations and give different NCP estimates, it still cannot reconcile discrepancy in NCPs (Text S2 and Table S2). Therefore, other processes must add nutrients or remove DIC, or a novel, unaccounted for mechanism is required to explain this disparity.

N_2 fixation could be one possible process providing new nitrogen to the system and would reconcile the inconsistency between the NCP estimates (Park et al., 2008). Recent studies have shown that N_2 fixation can occur at low temperatures and high latitudes (Harding et al., 2018; Sipler et al., 2017; Mills et al., 2018; Shiozaki et al., 2018), which challenges the historical views that N_2 fixation is a warm-water process constrained to subtropical and tropical oligotrophic areas (Zehr and Capone, 2020; von Friesen and Riemann 2020). Shiozaki et al. (2018) reported the N_2 fixation rates of 0.08 to 3.60 nmol N L^{-1} d^{-1} during late summer in 2015 in the Chukchi Sea, which is equivalent to 0.002 to 0.09 mmol N m^{-2} d^{-1} integrated over the top 25 m. Accounting for such a new source of nitrogen (using the upper limit), nNO_3^--based NCP would slightly increase by only ~2%, to 3.60 ± 0.07 and 5.15 ± 0.80 mmol N m^{-2} d^{-1} in the southern and northern Chukchi Sea, respectively (Table 5). Thus, N_2 fixation cannot explain the inconsistencies in NCP estimates based on the deficits of nDIC and nNO_3^-.

$CaCO_3$ formation or bio-calcification would also contribute to DIC removal in the water column. However, a net increase in nTA in both southern and northern Chukchi Sea (Table 5) suggests that $CaCO_3$ dissolution (e.g., mineral ikaite in ice) may dominate TA dynamics, which actually adds more DIC in the water column. By comparing the NCP results of with or without $CaCO_3$ dissolution correction, we further estimated that $CaCO_3$ dissolution accounted for ~2.6% and 11.0% $\text{NCP-}_{\text{nDIC based}}$ in the southern and northern Chukchi Seas, respectively, during the period between spring and early summer. Thus, $CaCO_3$ dissolution cannot explain the inconsistencies in NCP estimates either.

An alternative explanation is that, during intensive primary production, phytoplankton carbon and nutrient uptake in the Chukchi Sea are non-Redfieldian; DIC uptake exceeds that expected for the observed N and P uptake. Based on deficits of nDIC and nPO_4^{3-}, we found that C:P uptake ratio only slightly deviated from the Redfield ratio around 94.0 -128.0 (Table 5). Since the remaining PO_4^{3-} (~ 0.5 µM) would not limit phytoplankton growth, the inconsistency in NCP must be attributable to a non-Redfield C:N uptake behavior. We found that phytoplankton growth in a N-limited surface water led to a C:N uptake ratio of about 10.9-12.1 (Table 5), which is close to the measurements of the particulate organic C:N ratio in the Chukchi Sea in the summer of 2002 (C:N ratio > 9; Bates et al., 2005), but much higher than the Redfield ratio and the observed annual mean of particulate organic C:N ratio (~ 6.4; Frigstad et al., 2014). We attribute this disagreement to a rapid seasonal change in the phytoplankton C:N uptake ratio or an ecological response. The high NCP during late spring throughout early summer makes the Chukchi Sea an extremely NO_3^--limited ecosystem (Codispoti et al., 2013; Brown et al., 2015; Mills et al., 2015; Zheng et al., 2021), resulting in a higher C:N uptake ratio and hence a higher particulate organic C:N ratio (Bates et al., 2005). In contrast, the C:N uptake ratio is relatively low (close to the Redfield ratio) in early spring (Bates et al., 2005) and fall (Frigstad et al., 2014) when NO_3^- is replenished.

Additional evidence for C:N variability comes from water column-integrated NCP estimates. As phytoplankton growth and nutrient consumption may erode the nitricline, NCP calculated from surface water depletion of NO_3^- and DIC probably underestimates the true NCP or overestimates the C:N uptake ratio, we computed depth-integrated NCP for the entire water column. Previously, phytoplankton growth was observed in bottom waters in the southern Chukchi Sea in summers of 2010 and 2011 (Brown et al., 2015). In 2014, we observed excessive consumption of NO_3^- in bottom waters not only in the southern Chukchi Sea, but also in the northern part (Fig. 7 h; Fig. 12 b). The mean depth-integrated NCP in the southern and northern Chukchi Sea derived from nDIC changes were 65.4±46.7 and 98.7±55.8 mmol C m^{-2} d^{-1}, and NCP derived from nNO_3^- changes were 5.3±1.5 and 8.4±4.9 mmol N m^{-2} d^{-1}, respectively. These proportional increases in NCP estimates yield a C:N of 11.8 - 12.2, similar to that from the mixed layer analysis (Table S1), which confirms that C:N uptake ratio in the period between late spring and early summer was much higher than the Redfield ratio (C:N ~ 6.6). Given that nNO_3^- was still depleted in late summer and fall in the northern Chukchi Sea (Fig. 12 b), we further suggest that the C:N uptake ratio would remain high in the northern Chukchi Sea, while the C:N uptake ratio may return to the canonical Redfield ratio in the southern Chukchi Sea in the later season due to NO_3^- replenishment exceeding consumption (Frigstad et al., 2014; Zheng et al., 2021).

4.3 Flexible stoichiometric C:N uptake ratio enhances air-sea CO_2 uptake

The Chukchi Sea has been identified as a N-limited ecosystem during the growing season (Codispoti et al., 2013; Brown et al., 2015; Mills et al., 2015; Zhuang et al., 2020; Zheng et al., 2021). Thus, DIC assimilation and associated NCP calculation is directly linked to the uptake of the most limited nutrient (NO_3^-) and an assumption of a fixed C:N uptake ratio (Hansell et al., 1993; Arrigo et al., 2017). However, these assumptions are not always valid, especially when phytoplankton are experiencing N-limitation, because the internal C:N ratio of phytoplankton can deviate from the Redfield ratio (Finkel et al., 2010; Spilling et al., 2015) and the produced carbon-rich DOM can contribute a significant fraction of NCP (Bif and Hansell, 2019; Baetge et al., 2020). For example, when nutrients are sufficient, phytoplankton can assimilate and store extra nutrients for future use (i.e., luxury consumption; Elrifi and Turpin, 1985; Sommer, 1991). When nutrients in the internal pool or ambient water are not adequate, phytoplankton may release the fixed carbon as extracellular dissolved organic carbon (DOC) (Myklestad, 1995) or produce transparent exopolymeric particles (Vernet et al., 1998; Mari et al., 2001) and carbon-rich organic matter (Humphreys et al., 2019). From a biogeochemical perspective, this non-Redfield C:N uptake by phytoplankton may greatly impact seasonal variation in sea surface $p\mathrm{CO_2}$ and air-sea $\mathrm{CO_2}$ flux. For example, Fransner et al. (2018) found that $\mathrm{CO_2}$ uptake from the atmosphere can be underestimated by 50% in the northern Baltic Sea if a fixed Redfield ratio is used to determine carbon assimilation. However, there is little evidence for such a mechanism operating in the polar regions.

To demonstrate how a flexible C:N uptake stoichiometry by phytoplankton and possible $\mathrm{CaCO_3}$ dissolution during active ice melting affect the air-sea $\mathrm{CO_2}$ flux, we used a box model to reproduce sea surface $p\mathrm{CO_2}$ in the Chukchi Sea from spring to early summer in 2014. Three simulations were performed; scenario 1 with a non-Redfield C:N uptake ratio corrected for $\mathrm{CaCO_3}$ dissolution, scenario 2 with a non-Redfield C:N uptake ratio without correcting for $\mathrm{CaCO_3}$ dissolution and scenario 3 with a fixed Redfield C:N ratio (Fig. 13). In the simulation with a non-Redfield C:N uptake stoichiometry (scenario 1& 2), more efficient DIC drawdown led to a lower DIC concentration during early summer when compared to the Redfield ratio scenario, which results in better agreement with observations in both the southern and northern Chukchi Sea (Fig. 13 c and d). Furthermore, the non-Redfield stoichiometry approach better reproduces observations of $p\mathrm{CO_2}$ during this intensive growing season (Fig. 13 e and f), whereas carbon fixation in the fixed-stoichiometry (Redfield ratio) simulation is not efficient enough to counteract the effects of warming and air-sea $\mathrm{CO_2}$ exchange on sea surface $p\mathrm{CO_2}$. More importantly, the higher carbon fixation with a non-Redfield C:N uptake ratio, compared to the fixed Redfield uptake ratio, enhances air-sea $\mathrm{CO_2}$ uptake in the Chukchi Sea. The net $\mathrm{CO_2}$ uptake from the atmosphere in the non-Redfield stoichiometry scenario over the simulation period (day 136 to day 219 for the southern Chukchi Sea and day 167 to day 219 for the northern Chukchi Sea) is estimated to be 751 mmol C $\mathrm{m^{-2}}$ and 343 mmol C $\mathrm{m^{-2}}$, respectively, in the southern and northern Chukchi Sea, which are 42% and 85% higher than CO_2 uptake in the fixed-stoichiometry scenario (528 mmol C m^{-2} and 185 mmol C m^{-2}). Thus, we conclude that about 30% - 46% of CO_2 uptake during this intensive growing season is supported by phytoplankton stoichiometric flexibility. By comparing the results of scenarios 1 and 2, we further quantified that the correction of $CaCO_3$ dissolution during ice melting from spring to early summer accounted for ~1% and 9% CO_2 uptake in the southern and northern Chukchi Sea, respectively, which is a significant fraction of NCP estimate. The difference in the net uptake of atmospheric CO_2 between these simulations could increase as nutrient-limited conditions and high C:N uptake mechanisms extend to a longer growing season (e.g., late summer and fall).

5 Summary

Seasonality of biogeochemical properties determines how an ocean ecosystem responds to external and internal forcings. By synthesizing a rare dataset of underway measurements and discrete samples collected in five consecutive cruises in 2014, we presented a complete seasonal cycle (covering spring through fall) of sea surface $p$$CO_2$ and biogeochemical properties in the Chukchi Sea.

We first explored the dominant drivers of seasonal $p$$CO_2$ change as water masses evolve, revealing that thermal and non-thermal effects have different impacts on sea surface $p$$CO_2$ and air-sea CO_2 fluxes in different water masses. The non-ACW with stronger biological CO_2 removal and a weaker warming effect has a stronger atmospheric CO_2 uptake potential in summer months than ACW does. We suggest that the Chukchi Sea will become a greater CO_2 sink in the future as the proportion of nutrient-rich non-ACW increases.

We then estimated NCP for the most intensive growing period (spring to early summer) using observed DIC and nutrient data, and found that carbon-based NCP was consistently higher than NO_3^--based NCP by 66% - 84%. We attributed this inconsistency in NCP estimates to a non-Redfield uptake of carbon and nutrients.

To investigate this hypothesis, we performed two model simulations to test how a flexible stoichiometry of C:N uptake ratio can affect seasonal biogeochemical dynamics and air-sea CO_2

exchange. Comparing modeled results and observations, we show that a variable phytoplankton C:N stoichiometry is needed in order to better simulate and understand the seasonal biogeochemical dynamics and air-sea CO_2 exchange. In particular, this stochiometric flexibility in phytoplankton enables more efficient DIC-fixation, which contributes about 30% - 46% of CO_2 uptake from atmosphere in the Chukchi Sea. These model results also have important implications for biological pump estimates in the Chukchi ecosystem and parametrizing C and N cycles in regional biogeochemical models.

Acknowledgments: This work was supported by the United States National Science Foundation (PLR-1304337 and OPP-1926158), the US National Aeronautics and Space Administration (80NSSC22K0151), the National Key Research and Development Program of China (2019YFE0114800), the National Science Foundation of China (42176230, 41941013), the Green Network of Excellence (GRENE) Program/Arctic Climate Change Research Project, Arctic Challenge for Sustainability (ArCS; JPMXD1300000000) and Arctic Challenge for Sustainability II (ArCS II; JPMXD1420318865) Projects, which were funded by the Ministry of Education, Culture, Sports, Science and Technology of Japan (MEXT).

Author contributions: Conceptualization: Wei-Jun Cai, Zhangxian Ouyang, Andrew Collins; Data curation: Zhangxian Ouyang, Andrew Collins; Formal analysis: Zhangxian Ouyang; Funding acquisition: Wei-Jun Cai, Yun Li; Investigation: Di Qi, Kevin R. Arrigo, Yanpei Zhuang, Shigeto Nishino, Matthew P. Humphreys, Naohiro Kosugi, Akihiko Murata; Methodology: Zhangxian Ouyang; Resources: Liqi Chen, Jianfang Chen; Writing – original draft: Zhangxian Ouyang, Andrew Collins, Wei-Jun Cai; Writing – review & editing: Zhangxian Ouyang, Andrew Collins, Yun Li, Di Qi, Kevin R. Arrigo, Yanpei Zhuang, Shigeto Nishino, Matthew P. Humphreys, Naohiro Kosugi, Akihiko Murata, David L. Kirchman, Liqi Chen, Jianfang Chen, Wei-Jun Cai

Competing interests: The authors declare no competing interests.

Data Availability Statement: All the data are archived in publicly accessible databases. The SOCAT data can be downloaded from https://www.socat.info/index.php/data-access/. The data of discrete sample of carbonate chemistry, nutrients, dissolved oxygen and Chl *a* are also archived in publicly accessible databases (https://arcticdata.io/catalog/view/doi%3A10.18739%2FA21C1TG6R; https://data.mendeley.com/datasets/dfpxxwm24c/2; and http://www.godac.jamstec.go.jp/darwin/cruise/mirai/mr14-05/e). The model simulation data is also accessible via https://data.mendeley.com/datasets/xhj79xjhpc/1.

References

Anderson, L. G., Jutterström, S., Kaltin, S., Jones, E. P., & Björk, G. (2004). Variability in river runoff distribution in the Eurasian Basin of the Arctic Ocean. *Journal of Geophysical Research: Oceans*, 109(C1).

Armstrong, F., Stearns, C. R., & Strickland, J. (1967). The measurement of upwelling and subsequent biological process by means of the Technicon Autoanalyzer® and associated equipment. *Deep Sea Research*, 14, 381–389. https://doi.org/10.1016/0011-7471(67)90082-4

Ardyna, M., & Arrigo, K. R. (2020). Phytoplankton dynamics in a changing Arctic Ocean. *Nature Climate Change*, 10(10), 892-903.

Arrigo, K. R., & van Dijken, G. L. (2015). Continued increases in Arctic Ocean primary production. *Progress in Oceanography*, 136, 60-70.

Arrigo, K. R., Mills, M. M., van Dijken, G. L., Lowry, K. E., Pickart, R. S., & Schlitzer, R. (2017). Late spring nitrate distributions beneath the ice-covered northeastern Chukchi Shelf. *Journal of Geophysical Research: Biogeosciences*, 122(9), 2409-2417.

Baetge, N., Graff, J. R., Behrenfeld, M. J., & Carlson, C. A. (2020). Net community production, dissolved organic carbon accumulation, and vertical export in the Western North Atlantic. *Frontiers in Marine Science*, 7, 227.

Bakker, D. C., Pfeil, B., Landa, C. S., Metzl, N., O'brien, K. M., Olsen, A., ... & Xu, S. (2016). A multi-decade record of high-quality fCO 2 data in version 3 of the Surface Ocean CO 2 Atlas (SOCAT). *Earth System Science Data*, 8(2), 383-413.

Bates, N. R., Cai, W. J., & Mathis, J. T. (2011). The ocean carbon cycle in the western Arctic Ocean: Distributions and air-sea fluxes of carbon dioxide. *Oceanography*, *24*(3), 186-201.

Bates, N. R., Hansell, D. A., Moran, S. B., & Codispoti, L. A. (2005). Seasonal and spatial distribution of particulate organic matter (POM) in the Chukchi and Beaufort Seas. *Deep Sea Research Part II: Topical Studies in Oceanography*, 52(24-26), 3324-3343.

Bif, M. B., & Hansell, D. A. (2019). Seasonality of dissolved organic carbon in the upper Northeast Pacific Ocean. *Global Biogeochemical Cycles*, 33(5), 526-539.

Brewer, P. G., & Goldman, J. C. (1976). Alkalinity changes generated by phytoplankton growth. *Limnology and Oceanography*, 21(1), 108-117.

Brown, Z. W., Casciotti, K. L., Pickart, R. S., Swift, J. H., & Arrigo, K. R. (2015). Aspects of the marine nitrogen cycle of the Chukchi Sea shelf and Canada Basin. *Deep Sea Research Part II: Topical Studies in Oceanography*, 118, 73-87.

Buchanan, P. J., Matear, R. J., Chase, Z., Phipps, S. J., & Bindoff, N. L. (2018). Dynamic biological functioning important for simulating and stabilizing ocean biogeochemistry. *Global Biogeochemical Cycles*, 32(4), 565-593.

Buck, A. L. (1981). New equations for computing vapor pressure and enhancement factor. *Journal of Applied Meteorology and Climatology*, *20*(12), 1527-1532.

Cai, W. J., Chen, L., Chen, B., Gao, Z., Lee, S. H., Chen, J., ... & Zhang, H. (2010). Decrease in the CO2 uptake capacity in an ice-free Arctic Ocean basin. *Science*, 329(5991), 556-559.

Chen, B., Cai, W. J., & Chen, L. (2015). The marine carbonate system of the Arctic Ocean: assessment of internal consistency and sampling considerations, summer 2010. *Marine Chemistry*, 176, 174-188.

Clark, S. C., Granger, J., Mastorakis, A., Aguilar-Islas, A., & Hastings, M. G. (2020). An investigation into the origin of nitrate in Arctic sea ice. *Global Biogeochemical Cycles*, 34(2), e2019GB006279.

Codispoti, L. A., Kelly, V., Thessen, A., Matrai, P., Suttles, S., Hill, V., ... & Light, B. (2013). Synthesis of primary production in the Arctic Ocean: III. Nitrate and phosphate based estimates of net community production. *Progress in Oceanography*, 110, 126-150.

Comiso, J. C. (2017). Bootstrap Sea Ice Concentrations from Nimbus-7 SMMR and DMSP SSM/I-SSMIS, Version 3. Boulder, Colorado USA. NASA National Snow and Ice Data Center Distributed Active Archive Center. doi: https://doi.org/10.5067/7Q8HCCWS4I0R.

Cooper, L. W., McClelland, J. W., Holmes, R. M., Raymond, P. A., Gibson, J. J., Guay, C. K., & Peterson, B. J. (2008). Flow-weighted values of runoff tracers (δ18O, DOC, Ba, alkalinity) from the six largest Arctic rivers. *Geophysical Research Letters*, 35(18).

Corlett, W. B., & Pickart, R. S. (2017). The Chukchi slope current. *Progress in Oceanography*, 153, 50-65.

Dickson, A. G. (1996). Determination of dissolved oxygen in sea water by Winkler titration. WOCE Operations Manual (Volume 3, Section 3.1, Part 3.1.3 WHP Operations and Methods, WHP Office Report WHPO 91-1, WOCE Report No. 68/91, Nov. 1994, Revision 1, pp. 1–13). Woods Hole, MA. Retrieved from https://www.nodc.noaa.gov/woce/woce_v3/wocedata_1/whp/manuals/pdf/91_1/dick- son2.pdf

Dickson, A. G., Sabine, C. L., & Christian, J. R. (2007). Guide to best practices for ocean CO_2 measurements. North Pacific Marine Science Organization.

Elrifi, I. R., & Turpin, D. H. (1985). Steady-state luxury consumption and the concept of optimum nutrient ratios: A study with phosphate and nitrate limited Selenastrum minutum (chlorophyta) 1. *Journal of Phycology*, *21*(4), 592-602.

Evans, W., Mathis, J., Cross, J., Bates, N., Frey, K., Else, B., et al. (2015). Sea-air CO_2 exchange in the western Arctic coastal ocean. *Global Biogeochemical Cycles*, 29(8), 1190-1209. doi:10.1002/2015GB005153

Fetterer, F., K. Knowles, W. N. Meier, M. Savoie, and A. K. Windnagel. 2017, updated daily. Sea Ice Index, Version 3. Boulder, Colorado USA. NSIDC: National Snow and Ice Data Center. doi: https://doi.org/10.7265/N5K072F8.

Finkel, Z. V., Beardall, J., Flynn, K. J., Quigg, A., Rees, T. A. V., & Raven, J. A. (2010). Phytoplankton in a changing world: cell size and elemental stoichiometry. *Journal of plankton research*, 32(1), 119-137.

Fransner, F., Gustafsson, E., Tedesco, L., Vichi, M., Hordoir, R., Roquet, F., ... & Nycander, J. (2018). Non-Redfieldian Dynamics Explain Seasonal pCO_2 Drawdown in the Gulf of Bothnia. *Journal of Geophysical Research: Oceans*, *123*(1), 166-188.

Frigstad, H., Andersen, T., Bellerby, R. G., Silyakova, A., & Hessen, D. O. (2014). Variation in the seston C: N ratio of the Arctic Ocean and pan-Arctic shelves. *Journal of Marine Systems*, 129, 214-223.

Friis, K., Körtzinger, A., & Wallace, D. W. (2003). The salinity normalization of marine inorganic carbon chemistry data. *Geophysical Research Letters*, 30(2).

Gattuso J.-P., Epitalon J.-M., Lavigne H. & Orr J., 2018. seacarb: seawater carbonate chemistry. R package version 3.2.10. http://CRAN.R-project.org/package=seacarb

Gong, D., & Pickart, R. S. (2015). Summertime circulation in the eastern Chukchi Sea. *Deep Sea Research Part II: Topical Studies in Oceanography*, 118, 18-31.

Grebmeier, J. M., Bluhm, B. A., Cooper, L. W., Danielson, S. L., Arrigo, K. R., Blanchard, A. L., ... & Okkonen, S. R. (2015). Ecosystem characteristics and processes facilitating persistent macrobenthic biomass hotspots and associated benthivory in the Pacific Arctic. *Progress in Oceanography*, 136, 92-114.

Guo, L., Cai, Y., Belzile, C., & Macdonald, R. W. (2012). Sources and export fluxes of inorganic and organic carbon and nutrient species from the seasonally ice-covered Yukon River. *Biogeochemistry*, 107(1), 187-206.

Hansell, D. A., Whitledge, T. E., & Goering, J. J. (1993). Patterns of nitrate utilization and new production over the Bering-Chukchi shelf. *Continental Shelf Research*, 13(5-6), 601-627.

Harding, K., Turk-Kubo, K. A., Sipler, R. E., Mills, M. M., Bronk, D. A., & Zehr, J. P. (2018). Symbiotic unicellular cyanobacteria fix nitrogen in the Arctic Ocean. *Proceedings of the National Academy of Sciences*, 115(52), 13371-13375.

Humphreys, M. P., Achterberg, E. P., Hopkins, J. E., Chowdhury, M. Z., Griffiths, A. M., Hartman, S. E., ... & Moore, C. M. (2019). Mechanisms for a nutrient-conserving carbon pump in a seasonally stratified, temperate continental shelf sea. *Progress in Oceanography*, 177, 101961.

Holm-Hansen, O., Lorenzen, C. J., Holmes, R. W., & Strickland, J. D. H. (1965). Fluorometric determination of chlorophyll. ICES *Journal of Marine Science*, 30(1), 3–15. https://doi.org/10.1093/icesjms/30.1.3

Hydes, D. J., Aoyama, M., Aminot, A., Bakker, K., Becker, S., Coverly, S., et al. (2010). Determination of dissolved nutrients (N, P, Si) in seawater with high precision and inter-comparability using gas-segmented continuous flow analysers. In E. M. Hood, C. L. Sabine, & B. M. Sloyan (Eds.), The GO-SHIP Repeat Hydrography Manual: A Collection ofExpert Reports and Guidelines (IOCCP Report Number 14, ICPO Publication Series Number 134, pp. 1–87). Paris, France: UNESCO-IOC. Retrieved from http://www.go-ship.org/HydroMan.html, http://www.go-ship.org/Manual/Hydes_et_al_Nutrients.pdf

Jiang, L.-Q.**,** W.-J. Cai, and Y. Wang. 2008. A comparative study of carbon dioxide in river- and marine-dominated estuaries. *Limnology and Oceanography*, 53(6), 2603-2615.

Kawaguchi, Y., Nishino, S., & Inoue, J. (2015). Fixed-point observation of mixed layer evolution in the seasonally ice-free Chukchi Sea: Turbulent mixing due to gale winds and internal gravity waves. *Journal of Physical Oceanography*, 45(3), 836-853.

Kwiatkowski, L., Aumont, O., Bopp, L., & Ciais, P. (2018). The impact of variable phytoplankton stoichiometry on projections of primary production, food quality, and carbon uptake in the global ocean. *Global Biogeochemical Cycles*, 32(4), 516-528.

Koeve, W. (2006). C: N stoichiometry of the biological pump in the North Atlantic: Constraints from climatological data. *Global Biogeochemical Cycles*, *20*(3).

Lee, K. (2001). Global net community production estimated from the annual cycle of surface water total dissolved inorganic carbon. *Limnology and Oceanography*, 46(6), 1287-1297.

Lewis, K. M., G. L. van Dijken, and K. R. Arrigo. 2020. Changes in phytoplankton concentration now drive increased Arctic Ocean primary production. *Science*, 369: 198–202. doi:10.1126/science.aay8380

Li, M., Pickart, R. S., Spall, M. A., Weingartner, T. J., Lin, P., Moore, G. W. K., & Qi, Y. (2019). Circulation of the Chukchi Sea shelfbreak and slope from moored timeseries. *Progress in oceanography*, 172, 14-33.

Lin, P., Pickart, R. S., McRaven, L. T., Arrigo, K. R., Bahr, F., Lowry, K. E., et al. (2019). Water Mass Evolution and Circulation of the Northeastern Chukchi Sea in Summer: Implications for Nutrient Distributions. *Journal of Geophysical Research: Oceans*, 124(7), 4416–4432. https://doi.org/10.1029/2019JC015185

Lowry, K. E., Pickart, R. S., Mills, M. M., Brown, Z. W., van Dijken, G. L., Bates, N. R., & Arrigo, K. R. (2015). The influence of winter water on phytoplankton blooms in the Chukchi Sea. *Deep-Sea Research Part II: Topical Studies in Oceanography*, 118,53–72.

Mari, X., Beauvais, S., Lemée, R., & Pedrotti, M. L. (2001). Non-Redfield C: N ratio of transparent exopolymeric particles in the northwestern Mediterranean Sea. *Limnology and Oceanography*, 46(7), 1831-1836.

Martiny, A. C., Vrugt, J. A., Primeau, F. W., & Lomas, M. W. (2013). Regional variation in the particulate organic carbon to nitrogen ratio in the surface ocean. *Global Biogeochemical Cycles*, 27(3), 723-731.

Mathis, J. T., Bates, N. R., Hansell, D. A., & Babila, T. (2009). Net community production in the northeastern Chukchi Sea. *Deep Sea Research Part II: Topical Studies in Oceanography*, 56(17), 1213-1222.

Meredith, M. & Sommerkorn, M. IPCC Special Report on the Ocean and Cryosphere in a Changing Climate (SROCC), Chapter 3 (IPCC, Geneva, Switzerland, 2019).

Millero, F. J., Graham, T. B., Huang, F., Bustos-Serrano, H., & Pierrot, D. (2006). Dissociation constants of carbonic acid in seawater as a function of salinity and temperature. *Marine Chemistry*, 100(1-2), 80-94.

Mills, M. M., Brown, Z. W., Lowry, K. E., van Dijken, G. L., Becker, S., Pal, S., ... & Arrigo, K. R. (2015). Impacts of low phytoplankton NO3−: PO43− utilization ratios over the Chukchi Shelf, Arctic Ocean. *Deep Sea Research Part II: Topical Studies in Oceanography*, *118*, 105-121.

Mills, M. M., Brown, Z. W., Laney, S. R., Ortega-Retuerta, E., Lowry, K. E., Van Dijken, G. L., & Arrigo, K. R. (2018). Nitrogen limitation of the summer phytoplankton and heterotrophic prokaryote communities in the Chukchi Sea. *Frontiers in Marine Science*, *5*, 362.

Myklestad, S. M. (1995). Release of extracellular products by phytoplankton with special emphasis on polysaccharides. *Science of the total Environment*, *165*(1-3), 155-164.

Nishino, S., Kawaguchi, Y., Inoue, J., Hirawake, T., Fujiwara, A., Futsuki, R., ... & Aoyama, M. (2015). Nutrient supply and biological response to wind-induced mixing, inertial motion, internal waves, and currents in the northern C hukchi S ea. *Journal of Geophysical Research: Oceans*, *120*(3), 1975-1992.

Nishino, S., Kawaguchi, Y., Inoue, J., Yamamoto-Kawai, M., Aoyama, M., Harada, N., & Kikuchi, T. (2020). Do strong winds impact water mass, nutrient, and phytoplankton distributions in the ice-free Canada basin in the fall?. *Journal of Geophysical Research: Oceans*, 125(1), e2019JC015428.

Onarheim, I. H., Eldevik, T., Smedsrud, L. H., & Stroeve, J. C. (2018). Seasonal and regional manifestation of Arctic sea ice loss. *Journal of Climate*, 31(12), 4917-4932.

Ouyang, Z., Qi, D., Chen, L., Takahashi, T., Zhong, W., DeGrandpre, M. D., ... & Cai, W. J. (2020). Sea-ice loss amplifies summertime decadal CO_2 increase in the western Arctic Ocean. *Nature Climate Change*, 10(7), 678-684.

Ouyang, Z., Qi, D., Zhong, W., Chen, L., Gao, Z., Lin, H., ... & Cai, W. J. (2021). Summertime evolution of net community production and CO_2 flux in the western Arctic Ocean. *Global Biogeochemical Cycles*, 35(3), e2020GB006651.

Pacini, A., Moore, G. W. K., Pickart, R. S., Nobre, C., Bahr, F., Våge, K., & Arrigo, K. R. (2019). Characteristics and transformation of Pacific winter water on the Chukchi Sea shelf in late spring. *Journal of Geophysical Research: Oceans*, 124(10), 7153-7177.

Park, G. H., Lee, K., Wanninkhof, R., Zhang, J. Z., Hansell, D. A., & Feely, R. A. (2008). Large, non-Redfieldian drawdown of nutrients and carbon in the extratropical North Atlantic Ocean (46° N): Evidence for dinitrogen fixation?. *Limnology and oceanography*, 53(5), 1697-1704.

Pickart, R. S., Pratt, L. J., Torres, D. J., Whitledge, T. E., Proshutinsky, A. Y., Aagaard, K., ... & Dail, H. J. (2010). Evolution and dynamics of the flow through Herald Canyon in the western Chukchi Sea. *Deep Sea Research Part II: Topical Studies in Oceanography*, 57(1-2), 5-26.

Pickart, R. S., Nobre, C., Lin, P., Arrigo, K. R., Ashjian, C. J., Berchok, C., et al. (2019). Seasonal to mesoscale variability of water masses and atmospheric conditions in Barrow Canyon, Chukchi Sea. *Deep-Sea Research Part II: Topical Studies in Oceanography*,

Pierrot, D., Neill, C., Sullivan, K., Castle, R., Wanninkhof, R., Lüger, H., ... & Cosca, C. E. (2009). Recommendations for autonomous underway pCO2 measuring systems and data-reduction routines. *Deep Sea Research Part II: Topical Studies in Oceanography*, 56(8-10), 512-522.

Pisareva, M. N., Pickart, R. S., Lin, P., Fratantoni, P. S., & Weingartner, T. J. (2019). On the nature of wind-forced upwelling in Barrow Canyon. *Deep Sea Research Part II: Topical Studies in Oceanography*, 162,63–78. https://doi.org/10.1016/j.dsr2.2019.02.002

Redfield, A. C. (1958). The biological control of chemical factors in the environment. *American scientist*, 46(3), 230A-221.

Rysgaard, S., Glud, R. N., Sejr, M. K., Bendtsen, J., & Christensen, P. B. (2007). Inorganic carbon transport during sea ice growth and decay: A carbon pump in polar seas. *Journal of Geophysical Research: Oceans*, 112(C3).

Schlitzer, R. 2016. Ocean data view, DOI: 10.1098/rsta.2015. 0288.

Shiozaki, T., Fujiwara, A., Ijichi, M., Harada, N., Nishino, S., Nishi, S., ... & Hamasaki, K. (2018). Diazotroph community structure and the role of nitrogen fixation in the nitrogen cycle in the Chukchi Sea (western Arctic Ocean). *Limnology and Oceanography*, 63(5), 2191-2205.

Sipler, R. E., Gong, D., Baer, S. E., Sanderson, M. P., Roberts, Q. N., Mulholland, M. R., & Bronk, D. A. (2017). Preliminary estimates of the contribution of Arctic nitrogen fixation to the global nitrogen budget. *Limnology and Oceanography Letters*, 2(5), 159-166.

Sato, K., Aoyama, M., & Becker, S. (2010). Reference materials for nutrients in seawater as calibration standard solution to keep comparability for several cruises in the world ocean in 2000s. In M. Aoyama, A. G. Dickson, D. J. Hydes, A. Murata, J. R. Oh, P. Roose, & E. M. S. Woodward (Eds.), Comparability of nutrients in the world's ocean, (pp. 43–56). Tsukuba, Japan: Mother Tank.

Sommer, U. (1991). A comparison of the Droop and the Monod models of nutrient limited growth applied to natural populations of phytoplankton. *Functional Ecology*, 535-544.

Spilling, K., Ylöstalo, P., Simis, S., & Seppälä, J. (2015). Interaction effects of light, temperature and nutrient limitations (N, P and Si) on growth, stoichiometry and photosynthetic parameters of the cold-water diatom Chaetoceros wighamii. *PLoS One*, 10(5), e0126308.

Stabeno, P., Kachel, N., Ladd, C., & Woodgate, R. (2018). Flow patterns in the eastern Chukchi Sea: 2010–2015. *Journal of Geophysical Research: Oceans*, 123(2), 1177-1195.

Stroeve, J., & Notz, D. (2018). Changing state of Arctic sea ice across all seasons. *Environmental Research Letters*, 13(10), 103001.

Strong, A. L., Lowry, K. E., Brown, Z. W., Mills, M. M., van Dijken, G. L., Pickart, R. S., ... & Arrigo, K. R. (2016). Mass balance estimates of carbon export in different water masses of the Chukchi Sea shelf. *Deep Sea Research Part II: Topical Studies in Oceanography*, 130, 88-99.

Takahashi, T., Olafsson, J., Goddard, J. G., Chipman, D. W., & Sutherland, S. C. (1993). Seasonal variation of CO_2 and nutrients in the high-latitude surface oceans: A comparative study. *Global Biogeochemical Cycles*, 7(4), 843-878.

Takahashi, T., Sutherland, S. C., Wanninkhof, R., Sweeney, C., Feely, R. A., Chipman, D. W., ... & De Baar, H. J. (2009). Climatological mean and decadal change in surface ocean pCO2, and net sea–air CO2 flux over the global oceans. *Deep Sea Research Part II: Topical Studies in Oceanography,* 56(8-10), 554-577.

Tremblay, J. É., Anderson, L. G., Matrai, P., Coupel, P., Bélanger, S., Michel, C., & Reigstad, M. (2015). Global and regional drivers of nutrient supply, primary production and CO_2 drawdown in the changing Arctic Ocean. *Progress in Oceanography*, 139, 171-196.

Thoning, K., Crotwell, A., & Mund, J. (2021). Atmospheric Carbon Dioxide Dry Air Mole Fractions from continuous measurements at Mauna Loa, Hawaii, Barrow, Alaska, American

Samoa and South Pole. 1973-2020. Version 2021-08-09. National Oceanic and Atmospheric Administration (NOAA), Global Monitoring Laboratory (GML), Boulder, Colorado, USA, doi: https://doi. org/10.15138/yaf1-bk21.

Tu, Z., Le, C., Bai, Y., Jiang, Z., Wu, Y., Ouyang, Z., ... & Qi, D. (2021). Increase in CO_2 uptake capacity in the Arctic Chukchi Sea during summer revealed by satellite-based estimation. *Geophysical Research Letters*, e2021GL093844.

Vernet, M., Matrai, P. A., & Andreassen, I. (1998). Synthesis of particulate and extracellular carbon by phytoplankton at the marginal ice zone in the Barents Sea. *Journal of Geophysical Research: Oceans*, *103*(C1), 1023-1037.

von Friesen, L. W., & Riemann, L. (2020). Nitrogen fixation in a changing Arctic Ocean: An overlooked source of nitrogen?. *Frontiers in microbiology*, 11, 3149.

Wang, H., Lin, P., Pickart, R. S., & Cross, J. N. (2022). Summer surface CO2 dynamics on the Bering Sea and eastern Chukchi Sea shelves from 1989 to 2019. *Journal of Geophysical Research: Oceans*, 127(1), e2021JC017424.

Wanninkhof, R. (2014). Relationship between wind speed and gas exchange over the ocean revisited. *Limnology and Oceanography: Methods*, 12(6), 351-362.

Welschmeyer, N. A. (1994). Fluorometric analysis of chlorophyll a in the presence of chlorophyll b and pheopigments. Limnology and oceanography, 39(8), 1985-1992.

Weingartner, T., Aagaard, K., Woodgate, R., Danielson, S., Sasaki, Y., & Cavalieri, D. (2005). Circulation on the north central Chukchi Sea shelf. *Deep Sea Research Part II: Topical Studies in Oceanography*, 52(24-26), 3150-3174.

Weiss, R. (1974). Carbon dioxide in water and seawater: The solubility of a non-ideal gas. *Marine Chemistry, 2*(3), 203-215. doi:10.1016/0304-4203(74)90015-2

Woodgate, R. A., & Aagaard, K. (2005). Revising the Bering Strait freshwater flux into the Arctic Ocean. *Geophysical Research Letters*, 32(2).

Woodgate, R. A. (2018). Increases in the Pacific inflow to the Arctic from 1990 to 2015, and insights into seasonal trends and driving mechanisms from year-round Bering Strait mooring data. *Progress in Oceanography*, 160, 124–154. https://doi.org/10.1016/.pocean.2017.12.007

Woodgate, R. A., & Peralta-Ferriz, C. (2021). Warming and Freshening of the Pacific Inflow to the Arctic from 1990-2019 Implying Dramatic Shoaling in Pacific Winter Water Ventilation of the Arctic Water Column. *Geophysical Research Letters*, 48(9), e2021GL092528.

Yamamoto-Kawai, M., Tanaka, N., & Pivovarov, S. (2005). Freshwater and brine behaviors in the Arctic Ocean deduced from historical data of δ18O and alkalinity (1929–2002 AD). *Journal of Geophysical Research: Oceans*, 110(C10).

Yamamoto-Kawai, M., McLaughlin, F. A., Carmack, E. C., Nishino, S., & Shimada, K. (2008). Freshwater budget of the Canada Basin, Arctic Ocean, from salinity, δ18O, and nutrients. *Journal of Geophysical Research: Oceans*, 113(C1).

Zehr, J. P., & Capone, D. G. (2020). Changing perspectives in marine nitrogen fixation. *Science,* 368(6492).

Zheng, Z., Wei, H., Luo, X., & Zhao, W. (2021). Mechanisms of Persistent High Primary Production During the Growing Season in the Chukchi Sea. *Ecosystems*, 24(4), 891-910.

Zhuang, Y., Jin, H., Chen, J., Ren, J., Zhang, Y., Lan, M., ... & Tian, J. (2020). Phytoplankton community structure at subsurface chlorophyll maxima on the western Arctic shelf: patterns, causes, and ecological importance. *Journal of Geophysical Research: Biogeosciences*, 125(6), e2019JG005570.

Figure 1. Schematic circulation of the Chukchi Sea and the names of associated geographical locations (after Corlett & Pickart, 2017).

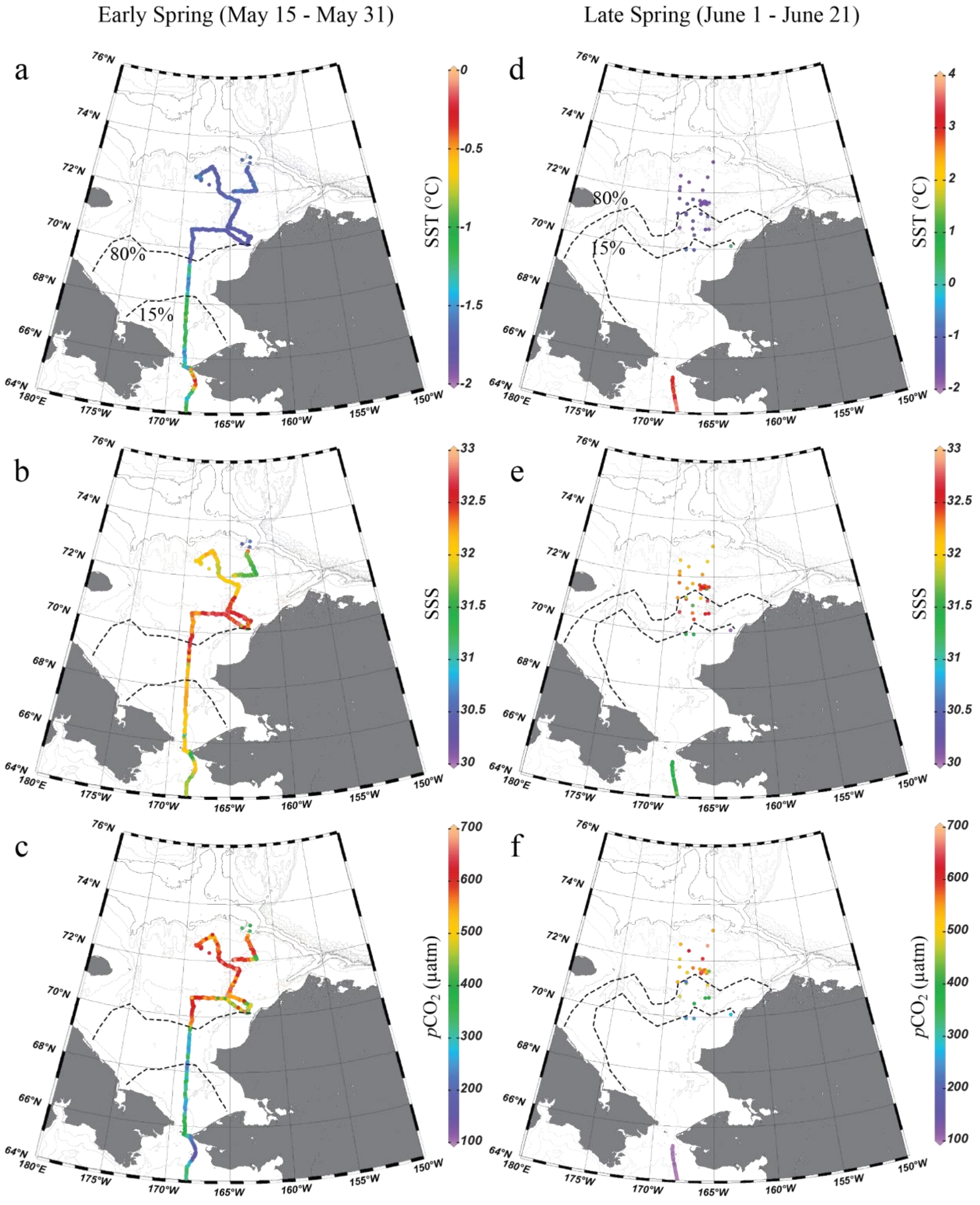

Figure 2. Sea surface temperature (SST), salinity (SSS), and pCO$_2$ in the spring of 2014 in the Chukchi Sea. The observations are presented in two periods, the early spring (May 15 - May 31)

and the late spring (June 1 - June 21). The dashed lines indicate the sea ice concentration contours of 15% and 80% on the last day of each period, May 31 (a-c) and June 21 (d-f), showing the possible maximum ice retreat for each period (National Snow and Ice Data Center, Fetterer et al., 2017, https://doi.org/10.7265/N5K072F8). Figures were created using Ocean Data View (Schlitzer 2016).

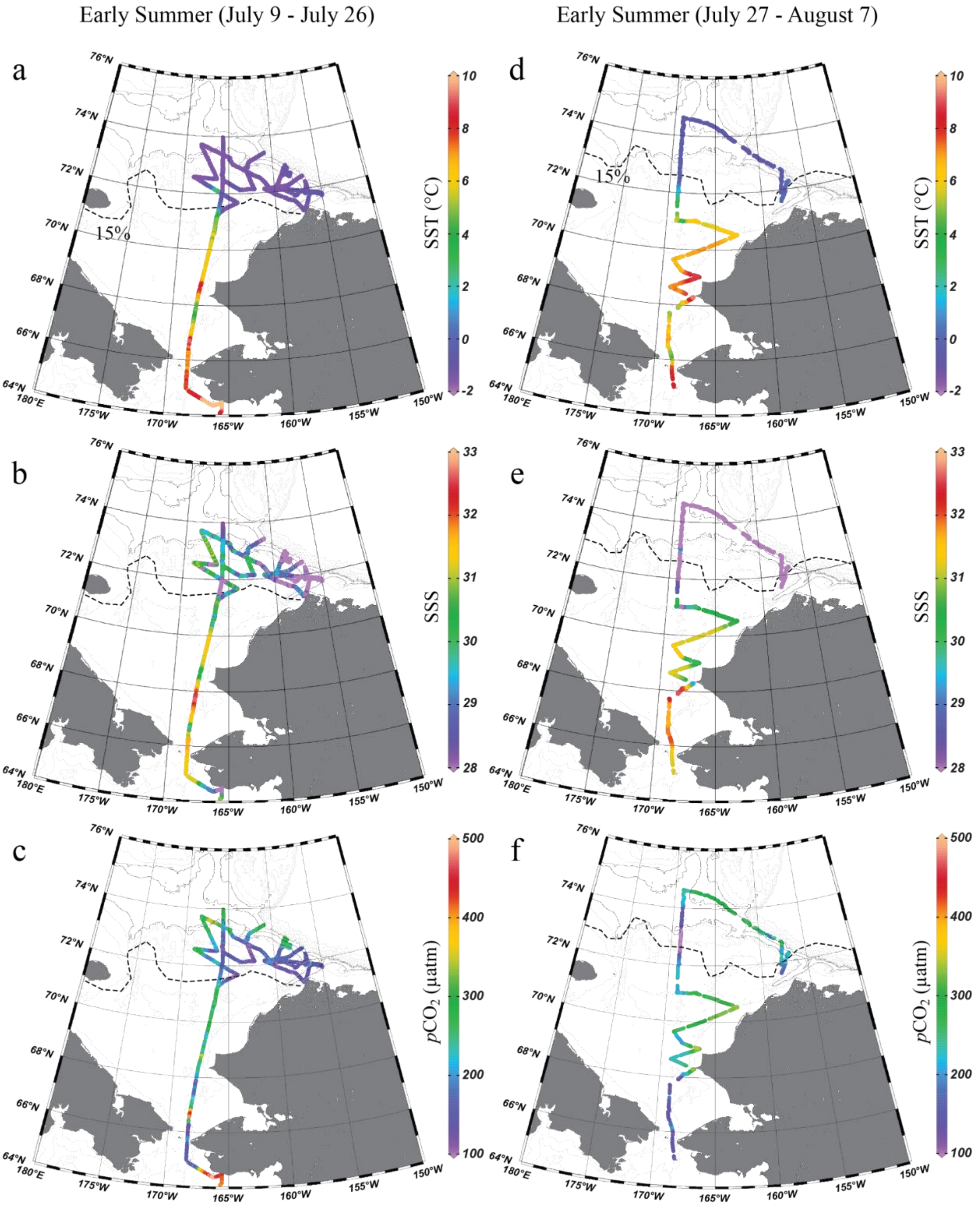

Early Summer (July 9 - July 26)

Early Summer (July 27 - August 7)

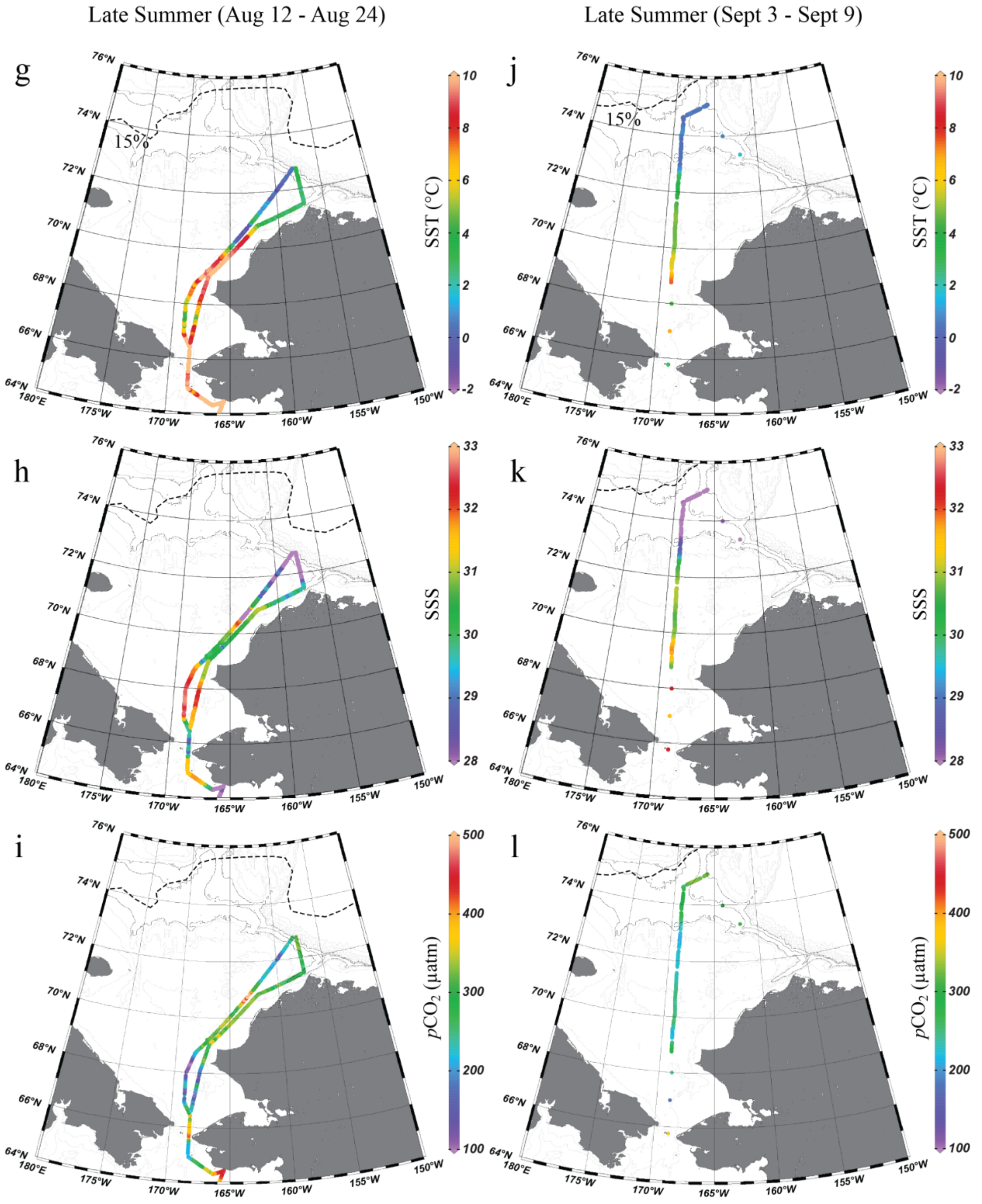

Figure 3. Sea surface temperature (SST), salinity (SSS), and pCO$_2$ in the summer of 2014 in the Chukchi Sea. The observations are presented in four periods depending on the timing of cruises,

July 9 - July 26 (a-c), July 27 - August 7 (d-f), August 12 - August 24 (g-i) and September 3 – September 9 (j-l). The dashed lines indicate the 15% sea ice concentration contour on the last day of each period, July 26 (a-c), August 7 (d-f), August 24 (g-i) and September 9 (j-l), showing the possible maximum ice retreat for each period (National Snow and Ice Data Center, Fetterer et al., 2017, https://doi.org/10.7265/N5K072F8). Figures were created using Ocean Data View (Schlitzer 2016).

Fall (Sept 25 - Sept 28)

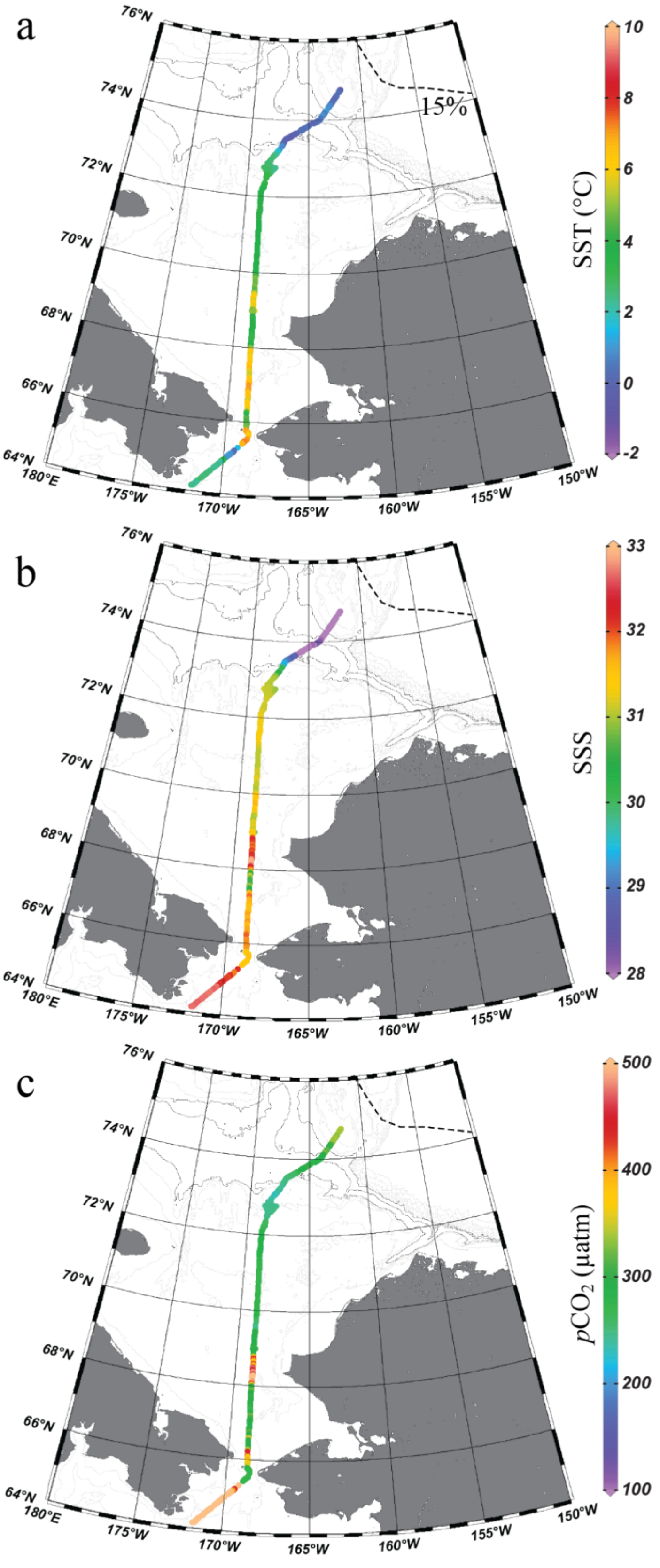

Figure 4. Sea surface temperature (SST), salinity (SSS), and pCO_2 in the fall of 2014 (September 25 – September 28) in the Chukchi Sea. The dashed lines indicate the 15% sea ice concentration contour on the last day of survey, September 28 (j-l), showing the possible maximum ice retreat for each period (National Snow and Ice Data Center, Fetterer et al., 2017, https://doi.org/10.7265/N5K072F8). Figures were created using Ocean Data View (Schlitzer 2016).

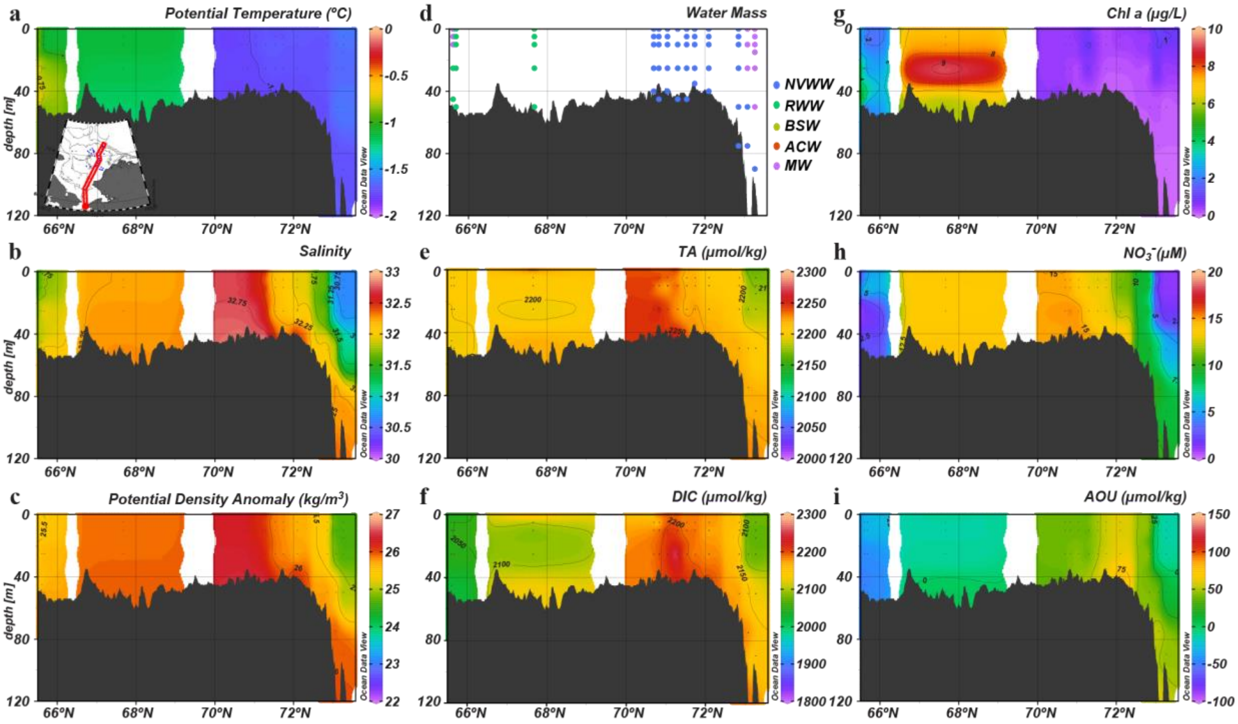

Figure 5. Vertical distributions of physical and biogeochemical parameters in the early spring (May 15 - May 31) along the central Chukchi Sea. (a) potential temperature, (b) salinity, (c) potential density anomaly, (d) water mass, (e) TA, (f) DIC, (g) chlorophyll *a*, (h) NO_3^- and (i) AOU.

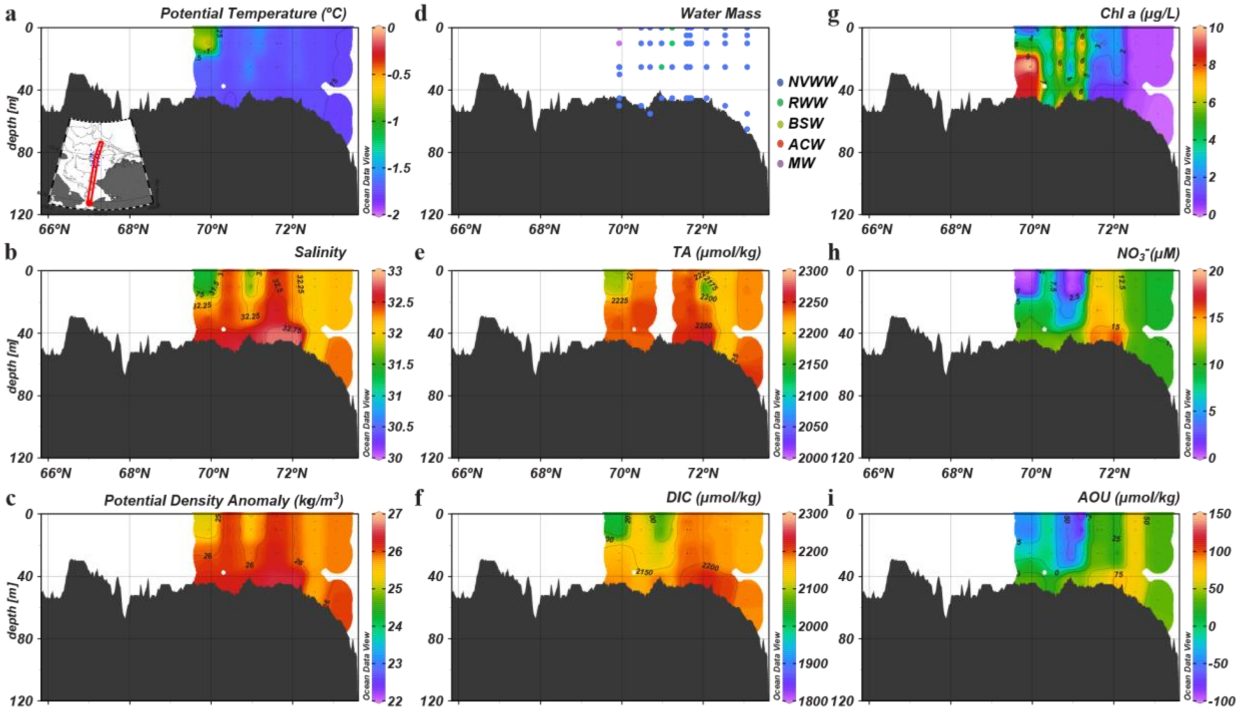

Figure 6. Vertical distributions of physical and biogeochemical parameters in the late spring (June 1 - June 21) along the central Chukchi Sea. (a) potential temperature, (b) salinity, (c) potential density anomaly, (d) water mass, (e) TA, (f) DIC, (g) chlorophyll *a*, (h) NO$_3^-$ and (i) AOU.

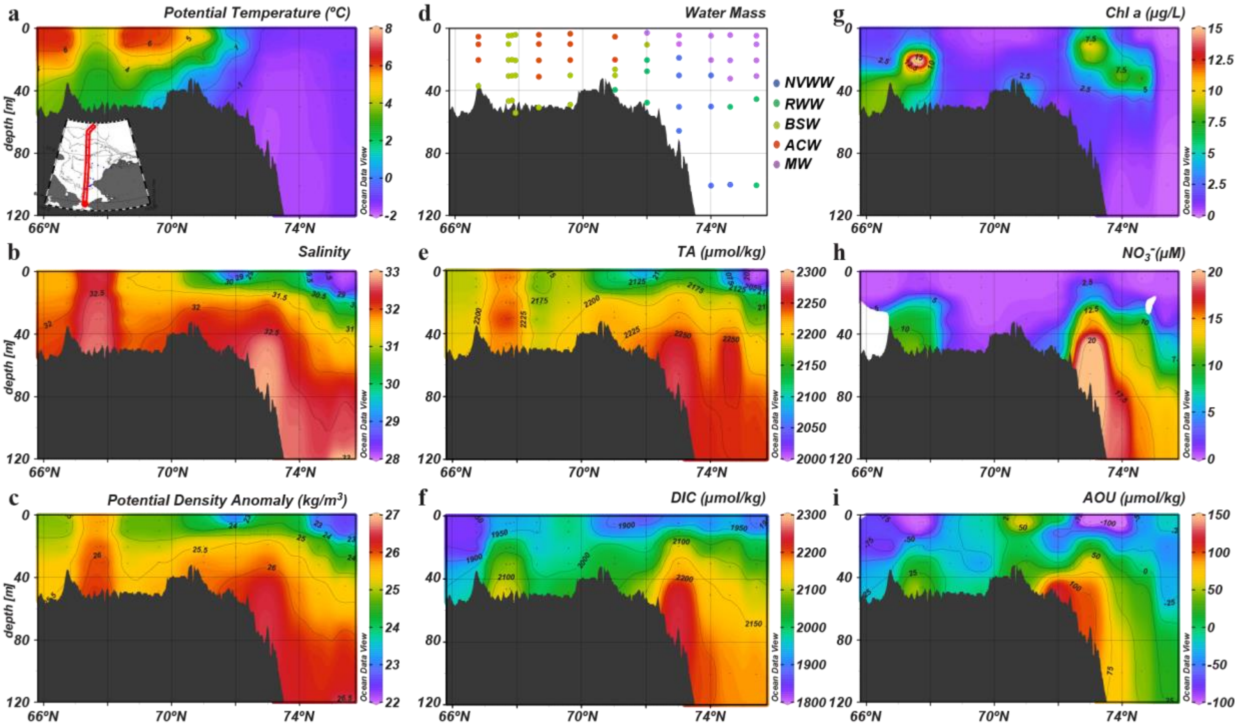

Figure 7. Vertical distributions of physical and biogeochemical parameters in the early summer (July 27 - August 7) along the central Chukchi Sea. (a) potential temperature, (b) salinity, (c) potential density anomaly, (d) water mass, (e) TA, (f) DIC, (g) chlorophyll *a*, (h) $\mathrm{NO_3^-}$ and (i) AOU. Note that the color scale of chlorophyll a concentration is different from that of Figs. 5h, 6h, and 9h.

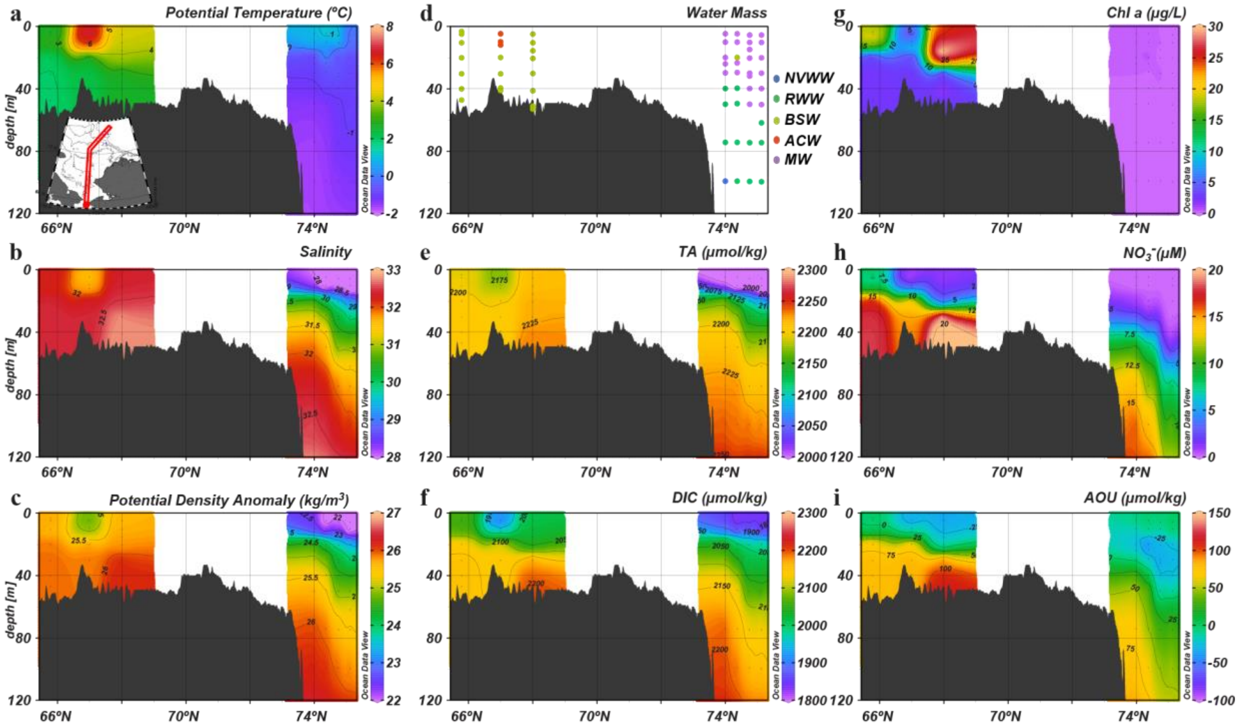

Figure 8. Vertical distributions of physical and biogeochemical parameters in the late summer (September 3 - September 9) along the central Chukchi Sea. (a) potential temperature, (b) salinity, (c) potential density anomaly, (d) water mass, (e) TA, (f) DIC, (g) chlorophyll *a*, (h) NO_3^- and (i) AOU. Note that the color scale of chlorophyll a concentration is different from that of Figs. 5h, 6h, and 9h.

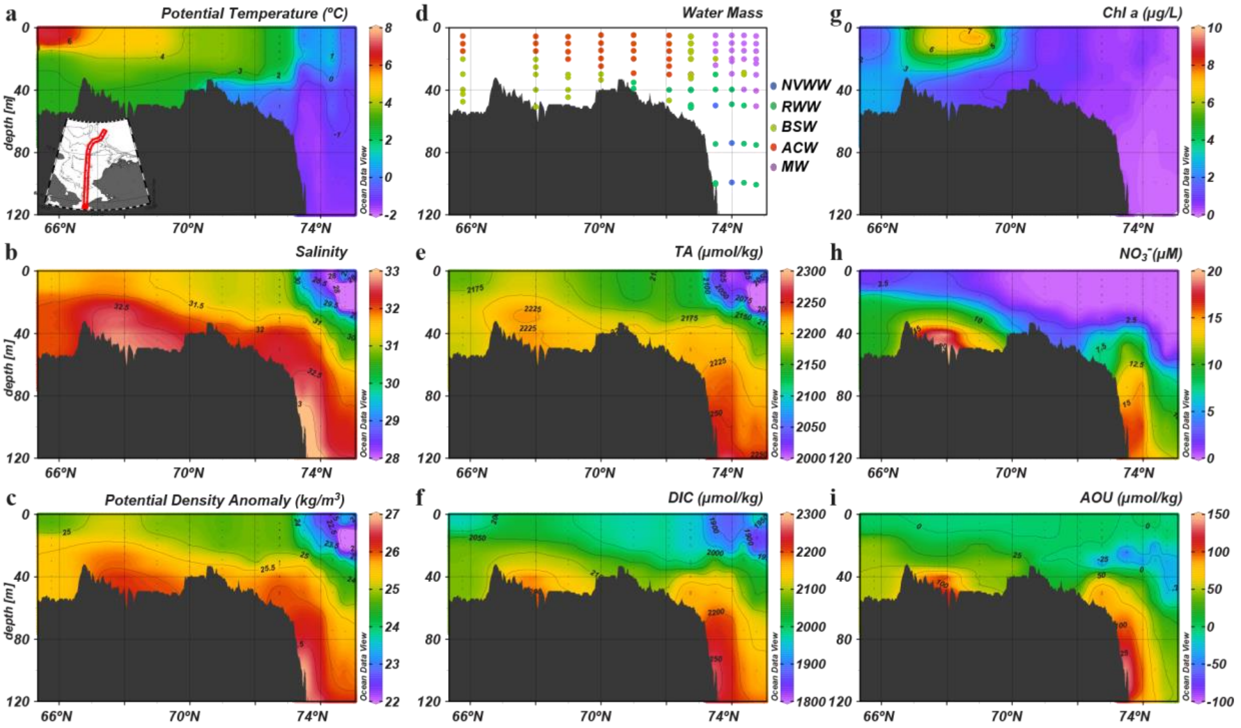

Figure 9. Vertical distributions of physical and biogeochemical parameters in the fall (September 24 - September 28) along the central Chukchi Sea. (a) potential temperature, (b) salinity, (c) potential density anomaly, (d) water mass, (e) TA, (f) DIC, (g) chlorophyll *a*, (h) NO_3^- and (i) AOU.

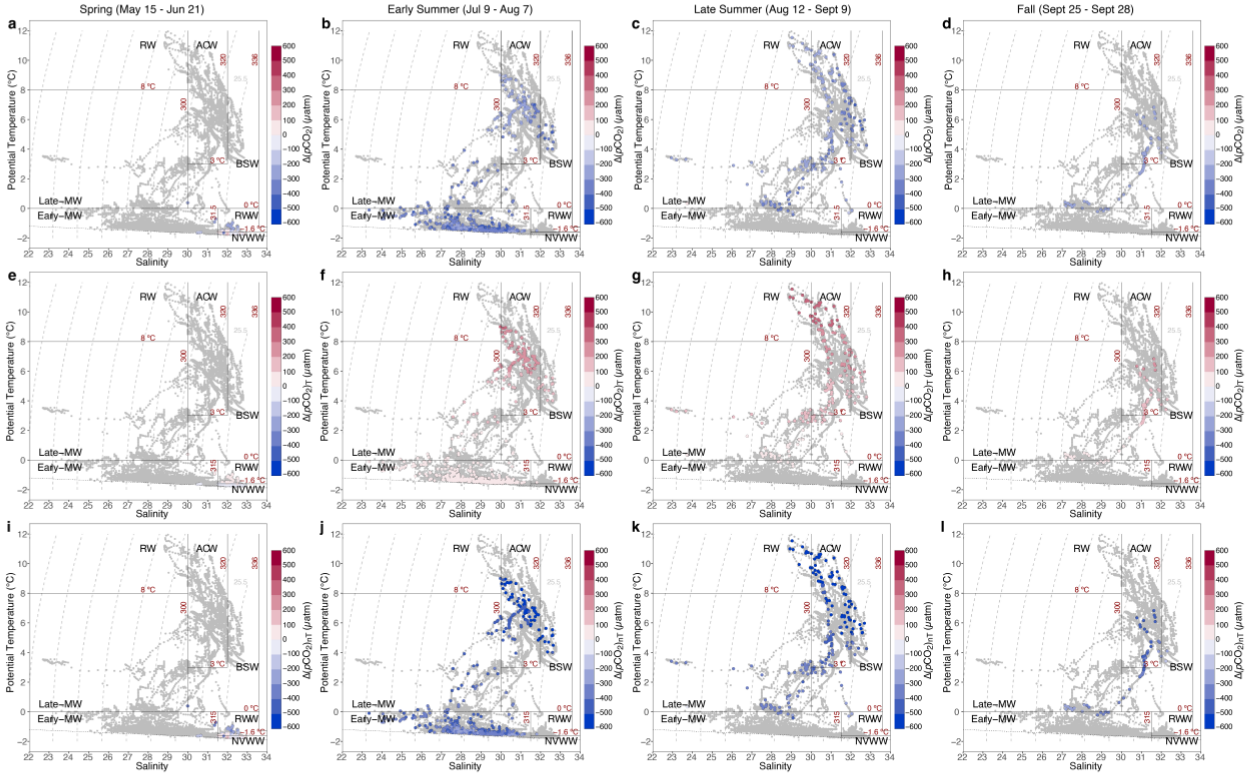

Figure 10. T/S diagram for sea surface pCO_2 in the Chukchi Sea in different seasons. The grey dots represent all underway measurements and colored dots denote the gridded pCO_2 (0.25º latitude × 0.25º longitude). (a-d) pCO_2 difference between initial pCO_2 under the ice (i.e., 538 µatm) and observed pCO_2, (e-g) potential pCO_2 changes induced by thermal effects, and (i-l) pCO_2 changes induced by non-thermal effects. The approximate water mass boundaries are denoted by solid lines. NVWW is newly-ventilated winter water; RWW is remnant winter water; BSW is Bering summer water; ACW is Alaskan coastal water; MW is meltwater; RW is river water. The freezing line is indicated by the dashed line.

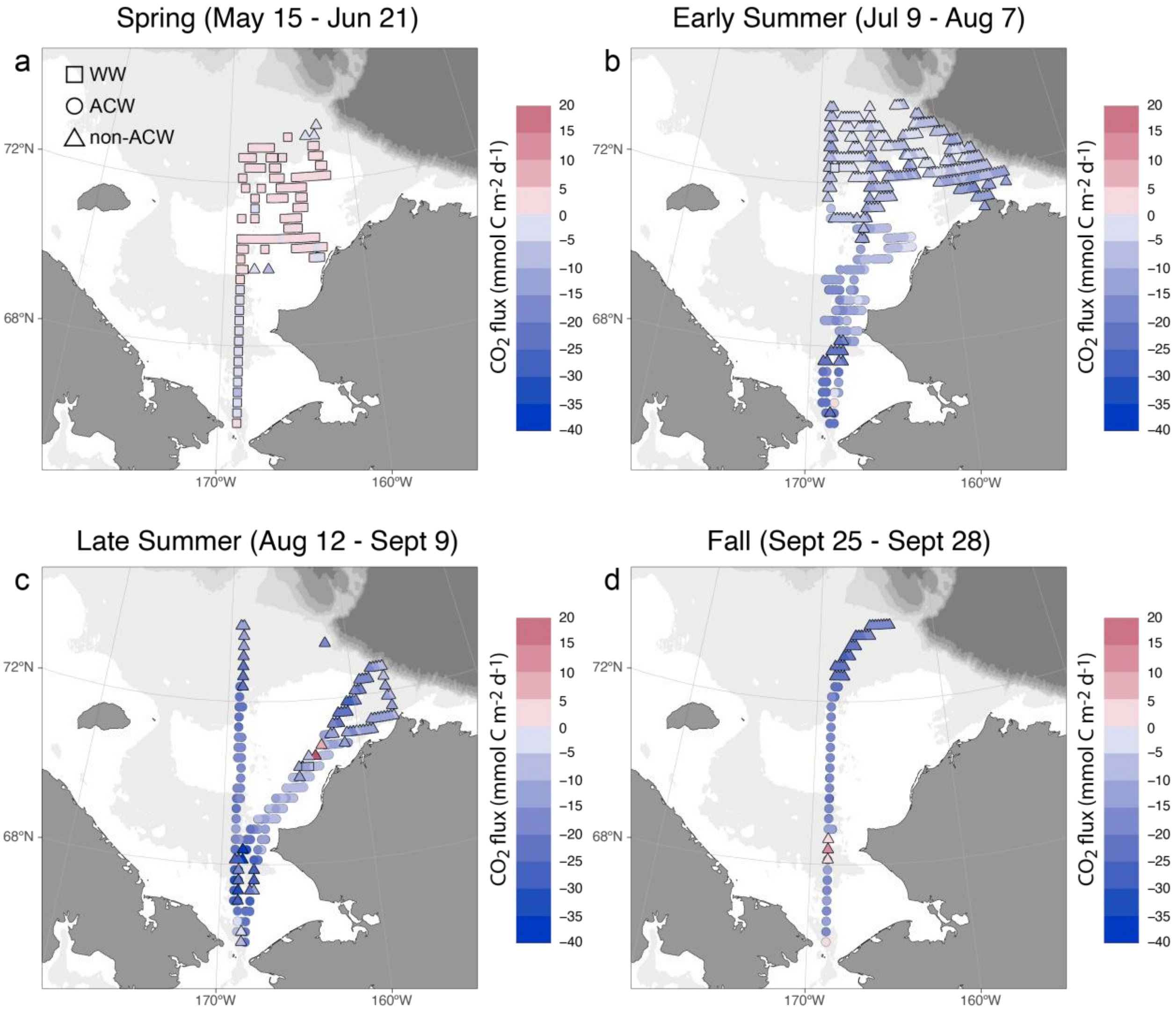

Figure 11. Seasonal variation in air-sea CO_2 flux in the Chukchi Sea in 2014. CO_2 flux were derived from gridded $p$$CO_2$ data (0.25º × 0.25º). Negative values of CO_2 flux values indicate that CO_2 uptake from the atmosphere. Square, circle and triangle represent winter water (NVWW and RWW), Alaska coastal water (ACW and RW), and non-Alaska coastal water (BSW and MW), respectively.

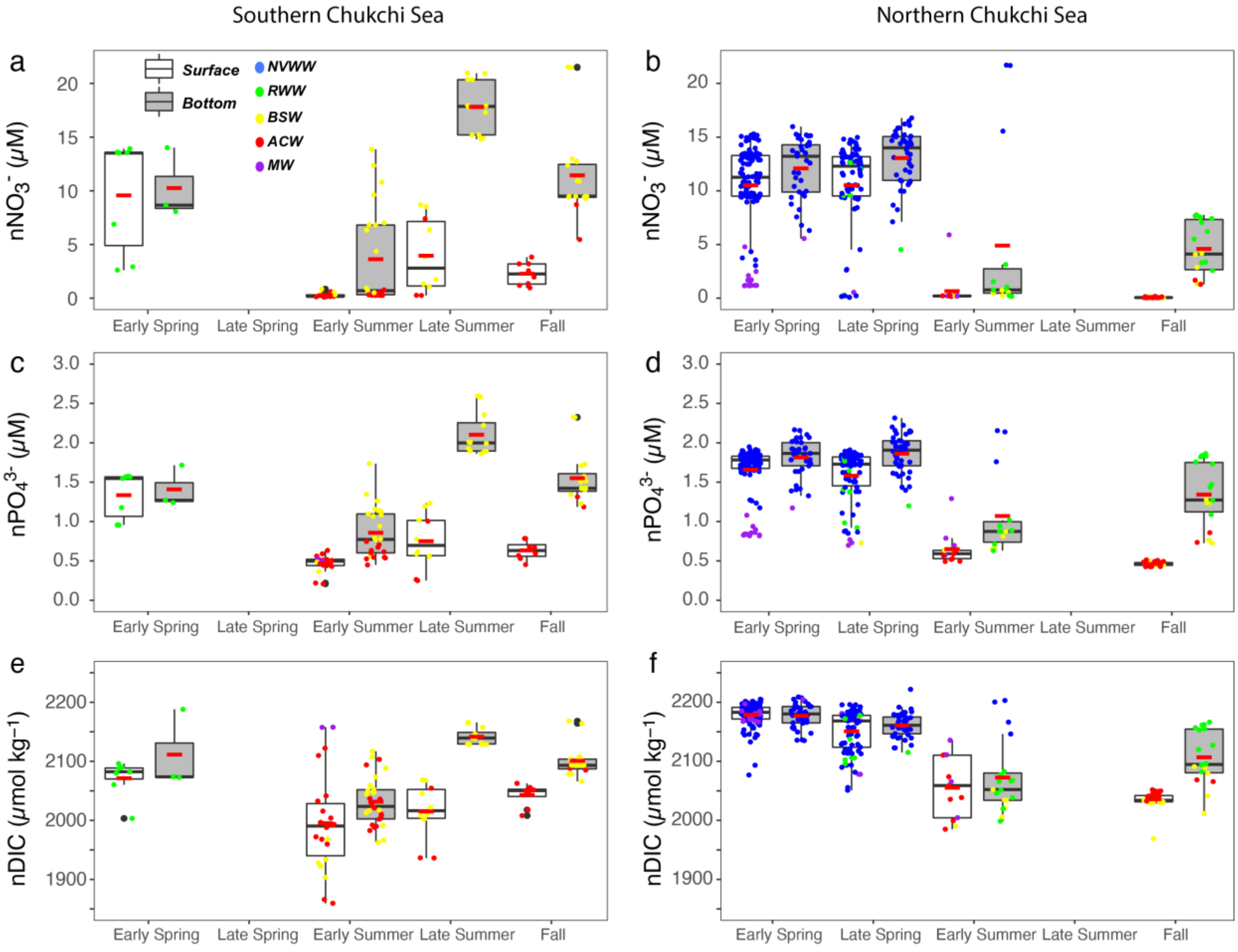

Figure 12. Seasonal variations of nNO_3^-, nPO_4^{3-}, and nDIC and in the southern (<69.5ºN; a, c, and e) and northern Chukchi Sea (>69.5ºN; b, d and f). White and grey boxplots indicate data collected in the surface and bottom layers, respectively. Black and red bars within boxplots indicate medians and means, respectively. Individual measurements are also shown and color-coded by different water masses.

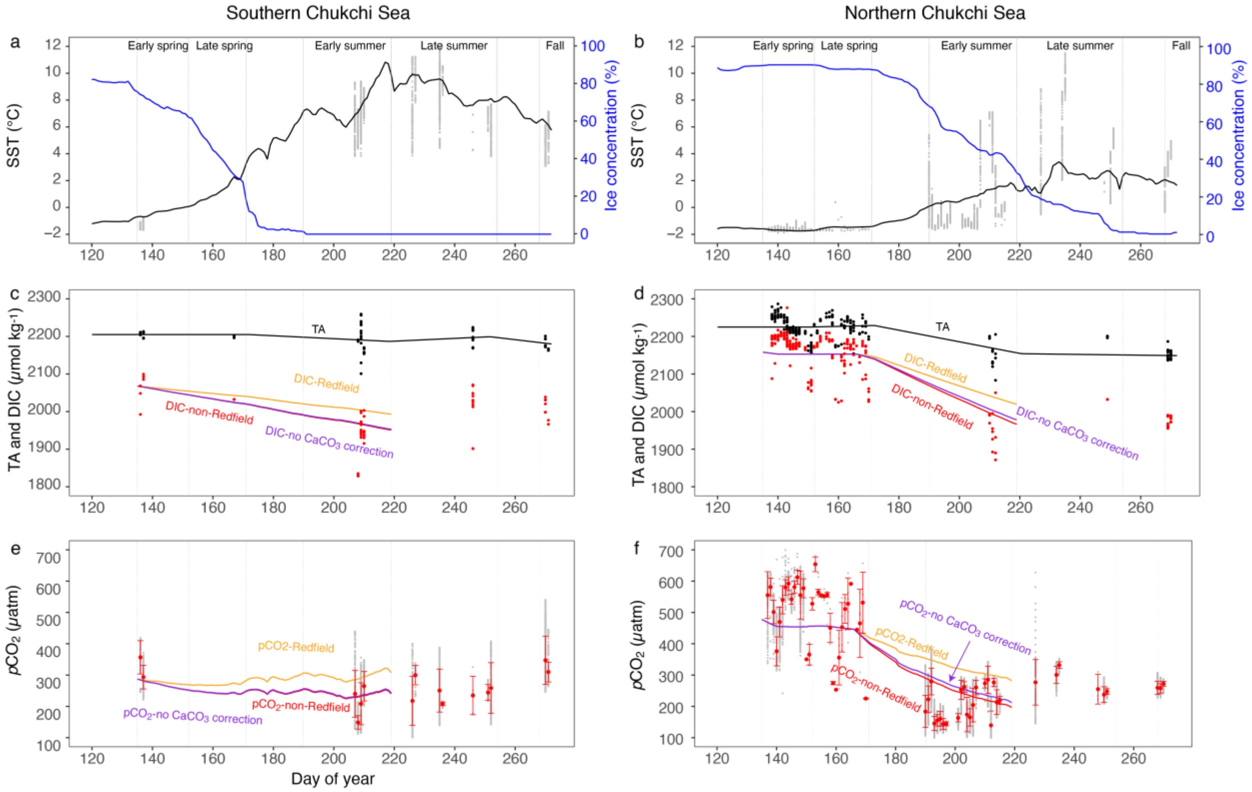

Figure 13. Observed and modeled seasonal variations in (a, b) SST and ice concentration, (c, d) TA and DIC, and (e, f) $p\mathrm{CO}_2$ in the southern Chukchi Sea (left column) and the northern Chukchi Sea (right column). The yellow lines are model results with fixed C:N uptake ratio (Redfield ratio). The red and purple lines indicate the model results with non-Redfield C:N uptake ratio with and without CaCO_3 dissolution correction, respectively. Black and red dots in c and d are discrete samples of TA and DIC, respectively. Grey dots are underway measurements of SST (a, b) and $p\mathrm{CO}_2$ (e, f). Daily means with error bar (±standard deviation) of underway $p\mathrm{CO}_2$ are presented in e and f. Five periods, including early and late spring, early and late summer, and fall are indicated by vertical dashed lines.

Table 1. Summary of cruises information and data sources.

Cruise	Period	Vessel	Data source of sea surface pCO_2	Data source of discrete samples
33HQ20140505	*Start:* 2014-05-05 *End:* 2014-06-21	Healy, USA	SOCATv2020	https://arcticdata.io/catalog/view/doi%3A10.18739%2FA21C1TG6R
33HQ20140709	*Start:* 2014-07-09 *End:* 2014-08-02	Healy, USA	SOCATv2020	No data collected
33HQ20140810	*Start:* 2014-08-10 *End:* 2014-08-29	Healy, USA	SOCATv2020	No data collected
76XL20140727	*Start:* 2014-07-27 *End:* 2014-09-09	Xuelong, China	SOCATv2020	https://data.mendeley.com/datasets/dfpxxwm24c/2
49NZ20140831	*Start:* 2014-09-03 *End:* 2014-09-28	Mirai, Japan	JAMSTEC	http://www.godac.jamstec.go.jp/darwin/cruise/mirai/mr14-05/e

Table 2. Definition of water masses in the Chukchi Sea.

Water masses		Temperature (℃)	Salinity
Newly-ventilated Winter Water	NVWW	T<-1.6 ℃	S>31.5
Remnant Winter Water	RWW	-1.6 ℃ < T < 0 ℃	S>31.5
Alaskan Coastal Water	ACW	T > 3.0 ℃	30< S <32
Bering Summer Water	BSW	0 ℃ < T < 3.0 ℃	30< S <33.6
		T > 3.0 ℃	32< S <33.6
Early-season Melt Water	ESMW	T < 0 ℃	S<31.5
Late-season Melt Water	LSMW	T > 0 ℃	S <30
River Water	RW	T > 8.0 ℃	S <30

Table 3. Seasonal variations in biogeochemical properties in the water column. Mean and standard deviation are reported for both the surface mixed layer and the bottom layer. No observations were made in the southern Chukchi Sea in late spring and in northern Chukchi Sea in late summer.

Periods	Layers	Temperature (℃)		Salinity		TA (μmol kg^{-1})		DIC (μmol kg^{-1})		AOU (μmol kg^{-1})		Chl *a* (μg l^{-1})		NO_3^- (μM)		PO_4^{3-} (μM)	
		Southern Chukchi	Northern Chukchi	Southern Chukchi	Northern Chukchi	Southern Chukchi	Northern Chukchi	Southern Chukchi	Northern Chukchi	Southern Chukchi	Northern Chukchi	Southern Chukchi	Northern Chukchi	Southern Chukchi	Northern Chukchi	Southern Chukchi	Northern Chukchi
Early spring	Surface	-1.28±0.19	-1.71±0.04	31.9 ±0.4	32.1±0.6	2205±7	2225±28	2068±35	2173±41	-13.9±3.5	35.6±23.2	4.4±3.1	0.9±1.7	9.57±5.29	10.54±3.95	1.33±0.30	1.66±0.32
	Bottom	-1.03±0.15	-1.74±0.04	32.2±0.3	32.4±0.4	2212±28	2236±18	2112±70	2191±27	-27.0±25.8	49.4±20.2	2.4±3.2	0.5±1.2	10.3±3.30	12.18±3.11	1.41±0.27	1.82±0.27
Late spring	Surface	NA	-1.61±0.36	NA	32.2±0.5	NA	2229±23	NA	2153±47	NA	14.3±38.0	NA	2.8±2.2	NA	10.57±4.33	NA	1.59±0.35
	Bottom	NA	-1.73±0.04	NA	32.6±0.2	NA	2243±13	NA	2188±23	NA	40.9±30.1	NA	2.9±3.1	NA	13.23±2.81	NA	1.89±0.26
Early Summer	Surface	5.95±1.80	3.76±2.79	31.4±1.0	30.7±0.9	2187±40	2154±37	1940±49	1954±51	-44.6±42.0	-8.2±59.5	1.4±1.2	1.8±3.2	0.27±0.20	0.62±1.51	0.46±0.11	0.62±0.20
	Bottom	3.93±1.61	-0.42±0.99	31.9±0.6	32.1±0.4	2204±31	2225±25	2015±64	2067±78	4.3±34.6	39.9±54.6	2.6±4.0	2.6±2.4	3.67±4.50	4.96±8.29	0.84±0.34	1.07±0.55
Late Summer	Surface	4.46±1.55	NA	32.1±0.3	NA	2199±20	NA	2012±61	NA	-16.6±17.1	NA	18.8±10.0	NA	3.95±3.46	NA	0.75±0.35	NA
	Bottom	2.27±0.27	NA	32.5±0.2	NA	2211±12	NA	2161±24	NA	88.5±13.7	NA	2.3±0.7	NA	18.01±2.53	NA	2.08±0.25	NA
Fall	Surface	5.33±0.99	3.10±0.58	31.6±0.2	31.1±0.2	2180±14	2149±12	2008±27	1971±13	-5.0±4.8	-4.4±11.4	5.8±2.9	0.7±0.4	2.24±1.07	0.06±0.03	0.62±0.12	0.45±0.03
	Bottom	3.15±0.37	0.66±1.56	32.4±0.4	32.2±0.3	2207±21	2208±15	2111±45	2105±59	44.7±32.0	35.1±48.7	2.2±1.1	0.6±0.3	11.53±4.48	4.60±2.51	1.56±0.35	1.34±0.41

Table 4. Seasonal variations in CO_2 flux (mmol m^{-2} d^{-1}) in the Chukchi Sea. We estimated CO_2 fluxes separately in two types of water masses: the ACW (including RW) and non-ACW (including BSW and MW but excluding NVWW and RWW) for each season.

	Southern Chukchi Sea (<69.5ºN)			Northern Chukchi Sea (>69.5ºN)		
Periods	Regional mean	ACW	Non-ACW	Regional mean	ACW	Non-ACW
Spring	-2.5±1.5 (n=15)	NA	NA	1.1±1.1 (n=145)	NA	-2.2±2.4 (n=6)
Early Summer	-15.9±6.0 (n=73)	-14.8±5.7 (n=62)	-22.3±1.9 (n=11) ***	-7.2±3.4 (n=377)	-8.8±2.6 (n=58)	-7.0±3.4 (n=319) ***
Late Summer	-18.3±8.9 (n=75)	-16.7±8.1 (n=59)	-24.3±9.6 (n=16) **	-13.3±6.6 (n=117)	-12.5±5.5 (n=54)	-14.2±7.4 (n-63)
Fall	-10.5±8.4 (n=17)	-13.7±4.4 (n=14)	4.4±6.1 (n=3) *	-21.1±2.9 (n=47)	-19.8±1.8 (n=15)	-21.7±3.2 (n=32) *

Note: Asterisk indicates if the mean of CO_2 flux in the non-ACW is statistically different from that in the ACW (t-test, *p < 0.05, **p< 0.01, ***p< 0.001).

Table 5. NCP estimates in the surface mixed layer based on nDIC, nNO_3^- and nPO_4^{3-} changes for the period between the late spring and the early summer of 2014 in the Chukchi Sea. Differences in nTA, nDIC, nNO_3^- and nPO_4^{3-} were calculated as $Variable_{spring}$ – $Variable_{early\ summer}$, thus negative values indicate an increase in variable in the later season. Nutrient-based NCP were converted to carbon (C) units assuming a Redfield molar C:N:P uptake ratio of 106:16:1. C:N and C:P uptake ratios are defined as NCP_{nDIC} : $NCP_{nNO_3^-}$ and NCP_{nDIC} : $NCP_{nPO_4^{3-}}$.

Location	Δ(nTA)	Δ(nDIC)	Δ(nNO_3)	Δ(nPO_4^-)	Growing season	N	NCP (nDIC based)	NCP (nNO_3^- based)		NCP (nPO_4^{3-} based)		C:N uptake ratio	C:P uptake ratio
	µmol kg^{-1}	µmol kg^{-1}	µM	µM	d		mmol C m^{-2} d^{-1}	mmol N m^{-2} d^{-1}	mmol C m^{-2} d^{-1}	mmol P m^{-2} d^{-1}	mmol C m^{-2} d^{-1}		
Southern	-34±37	79±87	10.24 ± 0.20	1.19±0.11	73	18	38.4 ± 26.2	3.51± 0.07	23.2 ± 0.5*	0.41±0.04	43.3 ± 4.0	10.9	94.0
Northern	-36±34	95±51	9.92±1.57	0.94±0.21	49	13	61.4 ± 20.0	5.06 ± 0.80	33.4 ± 5.3***	0.48±0.11	50.9 ± 11.3	12.1	128.0

Note: Asterisk indicates if the mean of $NCP_{nNO_3^-}$ and $NCP_{nPO_4^{3-}}$ in unit of mmol C m^{-2} d^{-1} are statistically different than that in NCP_{nDIC} (t-test, *p < 0.05, **p< 0.01, ***p< 0.001).